Arabian Journal of Chemistry (2020) 13, 7504–7523

King Saud University

Arabian Journal of Chemistry

www.ksu.edu.sa
www.sciencedirect.com

ORIGINAL ARTICLE

New anti-corrosion inhibitor (3ar,6ar)-3a,6a-di-p-tolyltetrahydroimidazo[4,5-d]imidazole-2,5(1 h,3h)-dithione for carbon steel in 1 M HCl medium: gravimetric, electrochemical, surface and quantum chemical analyses

Elyor Berdimurodov [a,*], Abduvali Kholikov [b], Khamdam Akbarov [b], Guobao Xu [c,d], Aboubakr M. Abdullah [e], Morteza Hosseini [f]

[a] *Faculty of Natural Sciences, Karshi State University, Karshi 180100, Uzbekistan*
[b] *Faculty of Chemistry, National University of Uzbekistan, Tashkent 100034, Uzbekistan*
[c] *State Key Laboratory of Electroanalytical Chemistry, Changchun Institute of Applied Chemistry, Chinese Academy of Sciences, Changchun, Jilin 130022, China*
[d] *University of Science and Technology of China, Hefei, China*
[e] *Center for Advanced Materials, Qatar University, Doha 2713, Qatar*
[f] *Department of Life Science Engineering, Faculty of New Sciences & Technologies, University of Tehran, Tehran 1417466191, Iran*

Received 11 July 2020; accepted 22 August 2020
Available online 28 August 2020

KEYWORDS

Corrosion;
Carbon steel;
Acid corrosion;
Acid inhibition;
Electrochemical calculation

Abstract The inhibition of (3ar,6ar)-3a,6a-di-p-tolyltetrahydroimidazo[4,5-d]imidazole-2,5(1 h,3 h)-dithione (TTHIIDT) for carbon steel was full characterized in a 1 M hydrochloride acid environment at various inhibitor concentrations and temperatures by the gravimetric, electrochemical, surface and quantum chemical analyses. The obtained results confirmed that the inhibition efficiency of TTHIIDT was over 95–97% and nearly stable in the rise of temperature and concentration; TTHIIDT was mixed type inhibitor and effectively influenced both anodic and cathodic corrosion reactions; a protective hydrophobic thin layer of this inhibitor on the carbon steel surface is more stable and non soluble in 1 M HCl medium; this inhibitor adsorbed endothermically on the carbon steel surface by the chemical and physical adsorption processes. The quantum chemical calculations

* Corresponding author at: Karshi State University, Department of Natural Science, Kashkadaryo Region, Karshi City, kuchabog 17, 180100, Uzbekistan.
E-mail address: elyor170690@gmail.com (E. Berdimurodov).
Peer review under responsibility of King Saud University.

Production and hosting by Elsevier

https://doi.org/10.1016/j.arabjc.2020.08.025

supported the experimental results and showed that the inhibition efficiency is depends on the structure of inhibitor.

1. Introduction

In the chemical industry, carbon steel is the dominant metal material because it is a low-cost and mechanically effective alloy. During the use of carbon steel in some processes, salt deposits and other corrosion products cover its surface. A 1 M HCl solution is used to remove the deposited salts from the metal surface; examples include the acid-pickling and oil well acidization metal-cleaning processes. Hydrochloride acid seriously damages the carbon steel surface, and this damage is responsible for the high-cost economic renovation and environmental problems. The most obvious way to address carbon steel destruction is by utilizing anti-corrosion inhibitors, which protect metals from aggressive corrosion attack in hydrochloride acid media. Presently, in corrosion science, pioneering effective, local-based, economic and environmentally friendly inhibitors is very important for solving corrosion problems in the chemical industry (Hou et al., 2020; Khalaf et al., 2020; Saleem Khan et al., 2020; Wang and Zhang, 2020).

It should be emphasized that in the literature, amine-, imidazoline-, surfactant- and polymer-based anti-corrosion inhibitors have been investigated. In the chemical industry, imidazole-based anti-corrosion inhibitors are mostly applied to protect carbon steel from corrosion attack. Recently, Chafiq et al. (2020) synthesised and investigated the benzimidazol based inhibitors for carbon steel, reported that these inhibitors are effective (93%) at 333 K. These inhibitors contains several sulfur, nitrogen and benzoyl rings, which make inhibitors to be good adsorbent. Chauhan et al. (2019) synthesised new biomacromolecule inhibitors based on triazole-modified chitosan, reported that this inhibitor is environmentally friendly and maximally protect (91.34% at 250 mg/L) steel materials from aggressive acidic corrosion. On the other hand, these inhibitors' efficiency degrees were reported to be just under 70–80% at low concentrations in aggressive acidic media, and some of them are more expensive and non-biodegradable and damage the local environment (Berdimurodov et al., 2017, 2018, 2019; Emoria et al., 2020; Eldesoky et al., 2020; Rauf and Mahdi, 2012).

In this research work, we have created a new imidazoline-based anti-corrosion inhibitor TTHIIDT, which is effective at low concentrations in a 1 M hydrochloride acid solution. There are some reasons for the selection of this inhibitor: first, it is synthesized based on local products, which makes it less expensive; second, this inhibitor is a biodegradable, non-toxic, water-soluble and good adsorbent on the surface of carbon steel. The anti-corrosion characteristics of the studied inhibitor were investigated by gravimetric, electrochemical, surface and quantum chemical analyses.

2. Experimental section

2.1. Carbon steel sample and investigated solution

In this research work, St2 steel material was used as a working electrode, which is manufactured by the "Chermetcom" trading company, Moscow, Russian Federation. St2 steel is a member of the carbon steel family and is mainly used in the chemical industry. It contains ~98% Fe, 0.09–0.15% C, 0.05–0.15% Si, 0.05% S, 0.25–0.5% Mn, 0.008% N, 0.04% P, 0.3% Cr, 0.3% Ni, 0.08% As and 0.3% Cu. The carbon steel material surface was cleaned and rubbed by SiC abrasive papers and then washed with distilled water, followed by ethanol and isopropyl alcohols. Last, it was dried with acetone. All experiments were carried out in 1 M hydrochloride acid solution, which was prepared from 36.5% HCl by diluting it with distilled water. The experiments were performed at inhibitor concentrations of 50, 100 and 150 mg/L. HCl (36.5%), thiourea and KOH were purchased from Tianjin Kemiou Chemical Reagent Co., Ltd., (P.R. China) and Tianjin Jiangtian Chemical Reagent Co., Ltd. (P.R. China).

2.2. The inhibitor TTHIIDT

In this research work, the inhibitor TTHIIDT was utilized, which was synthesized and characterized according to a previously reported synthetic methodology (Singh et al., 2014). The Scheme 1 represents that the molecular structure of the studied inhibitor.

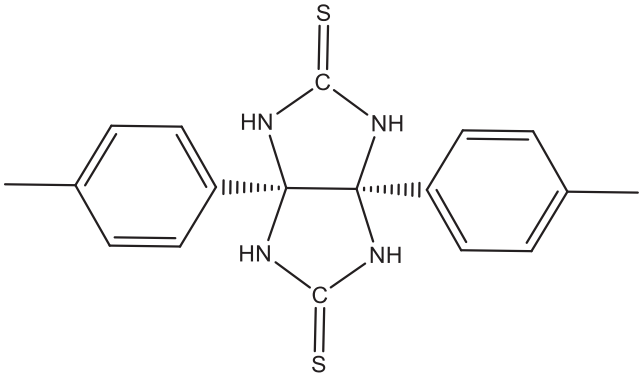

(3a*r*,6a*r*)-3a,6a-di-*p*-tolyltetrahydroimidazo[4,5-*d*]imidazole-2,5(1*H*,3*H*)-dithione

Scheme 1 The molecular structure of the inhibitor TTHIIDT.

2.3. Gravimetric analysis

In this investigation, gravimetric tests were conducted on 3 cm * 3 cm * 0.1 cm metal in the inhibitor-free and the inhibitor-containing 1 M HCl medium at various concentrations of the inhibitor TTHIIDT according to the ASTM G31-72 standard. The first step of the gravimetric tests was performed by immersing the studied metal sample for 3 h. In the following stage, this immersed metal sample was washed four times with distilled water and ethyl alcohol and then dried with acetone. In the final process, the dried metal sample weight was calculated three times, and the average weight was utilized for gravimetric measurements (Chauhan et al., 2020, 2019; Gupta et al., 2019; Fan et al., 2019; Kikanme et al., 2020; El Kacimi et al., 2020).

2.4. Electrochemical analysis

All electrochemical tests were performed by a Gamry potentiostat (IFC1000-06177)/(PC5) galvanostat/ZRA analyser (Model G-300, Pstat model Interface 1000, USA). To conduct the electrochemical tests, a three-electrode cell assembly was utilized, containing a working electrode (carbon steel sample), reference electrode (saturated calomel) and counter electrode (platinum). At the start of the electrochemical experiments, the three electrodes were submerged in the investigated solution, and the working electrode was immersed for 30 min. The diffusion potential of electrochemical processes on the surface of metal in solution changed for 30 min, after which it reached a stable state, indicating that the electrochemical processes on the surface of carbon steel in the studied environment achieved a steady-state potential. After 30 min of the diffusion-stabilization period, the open-circuit potentials were measured for 120 min because the quasi-substation processes on the surface of working carbon steel electrode stabilized and the OCPs reached a plateau. Finally, the corrosion parameters of the corrosion and inhibited media were measured by various electrochemical methods after a 150 min stabilization period (Chauhan et al., 2019; Gupta et al., 2019; Chafiq et al., 2020; Bahgat Radwan et al., 2017; Ye et al., 2020; Aly et al., 2020; Tabatabaei majd et al., 2020).

2.4.1. Electrochemical frequency modulation analysis

Electrochemical frequency modulation (EFM) experimental data were collected by EFM 140-Electrochemical frequency modulation software and analysed by Gamry Echem Analyst 6.22 software. In this research, a 10 mV amplitude potential perturbation signal and two 2 Hz and 5 Hz sine waves were used. This frequency choice gives several advantages: two frequencies (harmonic, intermodulation) cannot impact each other; the double-layer capacity on the steel surface slowly affects the frequency; and the frequency setting requires less time for performing the EFM experiment. The base frequency was 0.1 Hz. In the EFM tests, the intermodulation spectra have harmonic and intermodulation current peaks. In the Echem Analyst software, the corrosion current, corrosion rate, beta B (cathodic Tafel constant), beta A (anodic Tafel constant), causality factor (2) and (3) values were calculated by large harmonic and intermodulation current peaks in the EFM spectra (Al-Mobarak et al., 2011; Bosch et al., 2001; Berdimurodov, 2016; Obot and Onyeachu, 2018; Abdel-Rehim et al., 2006).

2.4.2. Electrochemical noise analysis

In this research work, the electrochemical noise analysis data were measured by EN120 electrochemical noise Gamry Framework 6.22 and Gamry Echem Analyst 6.22 software. In the electrochemical noise analyses, the ZRA control mode, the anodic current convention, and the following setup parameters were selected: the block time is 4 sec, the sample period is 0.05 sec, repeat time is 0.25 min and total time is 0.5 h (Danaee et al., 2019; Obot et al., 2019; Ramezanzadeh et al., 2014; Naghizade et al., 2020; Hou et al., 2016; Huet and Ngo, 2019; Ehsani et al., 2017).

2.4.3. Potentiodynamic polarization analysis

In this research paper, potentiodynamic polarization (PDP) analyses were applied to test the inhibition behaviour of the studied steel working electrode in an aggressive 1 M HCl medium and an inhibited environment. The PDP data were obtained by using the DC 105 corrosion Gamry Framework 6.22 and Gamry Echem Analyst 6.22 software. The PDP examinations were carried out within a −0.250 to 0.250 V potential range with a 1 mV/s scan rate and 2 sec sample period, starting the scans at the open-circuit potential (Gupta et al., 2019; Chafiq et al., 2020; Bahgat Radwan et al., 2017; Rbaa et al., 2020; Tan et al., 2020a, 2020b; El Kacimi et al., 2020; Ye et al., 2020; Aly et al., 2020).

2.4.4. Electrochemical impedance spectroscopy analysis

Electrochemical impedance spectroscopy (EIS) analyses were used utilising Gamry EIS300-Electrochemical Impedance software at 10 mV_{rms} AC voltage amplitude and open-circuit potential with frequencies among 100 kHz and 0.01 Hz. The EIS electrochemical behaviour of the studied metal specimen in the corrosive and inhibited media were measured by fitting the EIS Bode and Nyquist plots with Gamry Echem Analyst 6.22 software (Chauhan et al., 2020, 2019; Gupta et al., 2019; Kikanme et al., 2020; El Kacimi et al., 2020; Ye et al., 2020; Aly et al., 2020).

2.5. Surface analysis

The surface characteristics of investigated metal specimen in a 1 M hydrochloride acid environment with and without the inhibitor TTHIIDT at the optimum concentration was researched by scanning electron microscopy (SEM) on a HITACHI TM3000 system. Before taking SEM images, the metal was immersed for 3 h in the studied solutions. After immersion, the specimen was washed four times with distilled water and alcohol. In the final step, is the specimen was dried with acetone followed by SEM measurement (El Kacimi et al., 2020; Ye et al., 2020; Aly et al., 2020; Tabatabaei majd et al., 2020; Dehghani et al., 2020; Lgaz et al., 2020).

2.6. Quantum chemical analysis

To exam the quantum chemical properties of the inhibitor TTHIIDT, the quantum computation was conducted through density functional theory (DFT). The B3LYP method was per-

formed in the DFT calculations with 6-311G (d, p) basis sets. The DFT analysis illustrated the correlation between the inhibition properties and the molecular characteristics of the investigated inhibitor (Gupta et al., 2019; Chafiq et al., 2020; Bahgat Radwan et al., 2017; Rbaa et al., 2020; Tan et al., 2020).

3. Results and discussion

3.1. Gravimetric measurements

3.1.1. Concentration influence

To identify the impact of the TTHIIDT concentration on the inhibition efficiency, the gravimetric analysis was performed at constant temperature (303 K) with various concentrations, as described in Fig. 1(a). The inhibition efficiencies and corrosion rates at given concentrations were derived according to Equations (1) and (2), respectively.

$$\eta_{Grav.}, \% = (1 - \frac{W_{inh}}{W_0}) \times 100 \quad (1)$$

where $\eta_{Grav.}$ is the inhibition efficiency degree, and W_{inh} and W_0 represent the mass loss of the studied metal sample in inhibited and uninhibited 1 M HCl solutions.

$$CR_{Grav.} = \frac{W}{At} \quad (2)$$

where $CR_{Grav.}$ symbolizes the corrosion rate at mg/cm^{2}hour, A demonstrates the surface area in cm^2, t represents the immersion time in hours and W indicates the weight loss, respectively (Chauhan et al., 2019; Gupta et al., 2019; Chafiq et al., 2020; Bahgat Radwan et al., 2017; Rbaa et al., 2020).

Generally, it should be stressed from Fig. 1(a) that the corrosion rate of a given metal sample and the inhibition efficiency of the observed inhibitor slowly increased and then reduced with rising inhibitor concentrations at a given constant temperature. Correspondingly, at 150 mg/L concentration of the inhibitor TTHIIDT, it was recorded that $CR_{Grav.}$ was 0.012 mg/cm^{2}hour and that $\eta_{Grav.}$ was 99.15%. This phenomenon occurred because of the electron-rich sulfur and nitrogen heteroatoms in the inhibitor TTHIIDT, which promoted better adsorption interactions, in addition to the π-electron donor phenyl rings, which also supported those interactions.

3.1.2. Temperature influence

Temperature is an important element that changes the corrosion characteristics of carbon steel surfaces; it can influence all electrochemical corrosion mechanism processes on carbon steel surfaces. As a basic framework for analysing the thermo-inhibition behaviour of the inhibitor TTHIIDT at 303–333 K, in the inhibited and uninhibited 1 M hydrochloride medium, the inhibition efficiency and corrosion rate were measured, and the observed data are presented in Table 1. As

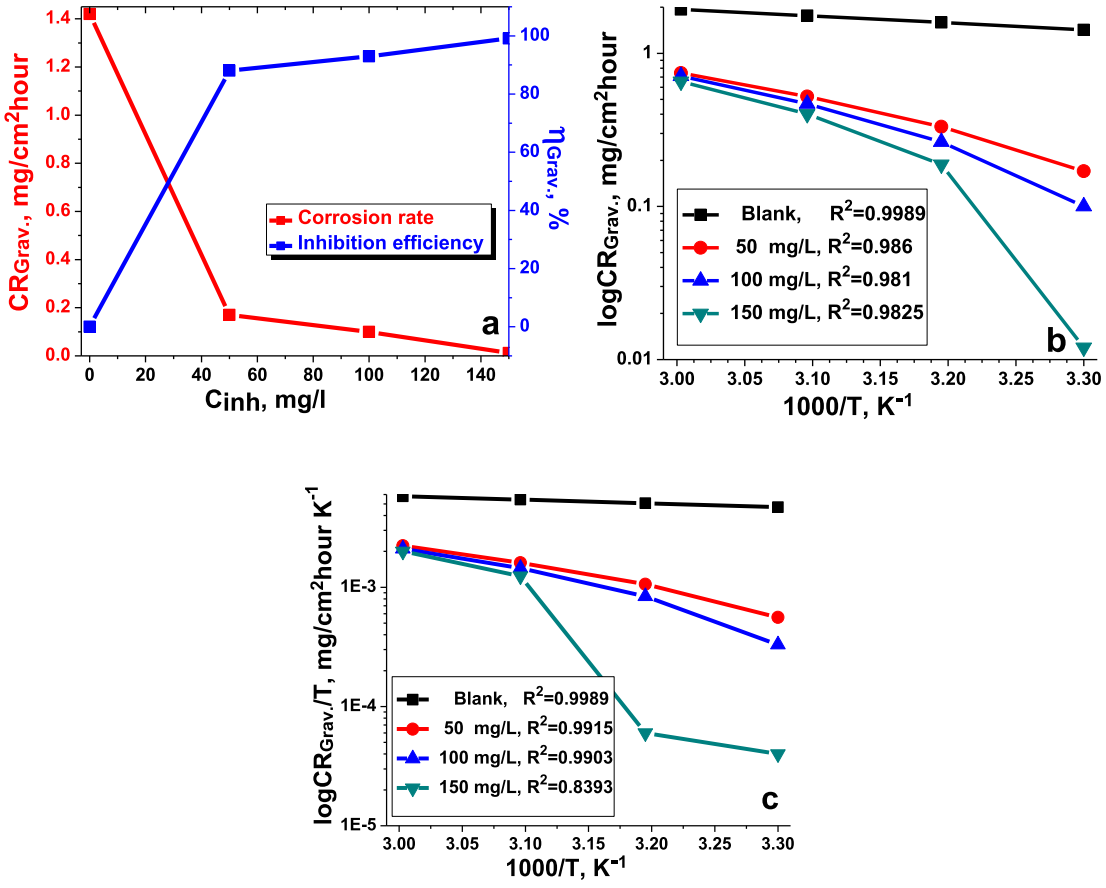

Fig. 1 Concentration versus inhibition efficiency and corrosion rate (a) (303 K), Arrhenius (b) and transition-state plots (c) for carbon steel in the inhibitor-free and the inhibitor-containing 1 M HCl medium at different concentrations of the inhibitor TTHIIDT.

shown from the obtained data, the corrosion rate considerably rose with increasing temperature, suggesting that the surface of carbon steel was more dissolved in a given acid solution; for instance, at 333 K, the corrosion rates were 1.93 and 0.6546 mg/cm^{2}hour in the inhibitor-free and inhibitor-containing media, respectively. On the other hand, it was reported that the inhibition efficiency slowly reduced as the temperature rose, reflecting that the studied inhibitor adsorption capacitance and inhibition efficiency depend on the temperature change. The decrease in the inhibition efficiency with rising temperature is due to desorption of the inhibitor from the steel surface at higher temperatures. This effect is due to the breaking of bonds between the inhibitor and the steel surface which releases the inhibitor back into solution and exposed the steel surface to corrosion.

3.1.3. Thermodynamics of activation

The thermodynamic behaviour of activated adsorption processes in the inhibitor-free and inhibitor-containing 1 M hydrochloride acid solutions were studied by gravimetric analysis. The temperature was a key factor in determining the thermodynamic parameters of the studied system in this research work, and the relationship between the temperature and corrosion rate could be illustrated according to the Arrhenius equation (Equation (3)).

$$CR_{Grav.} = A\exp\left(\frac{-E_a}{RT}\right) \tag{3}$$

where T demonstrates the temperature in K, E_a is the energy of activation in kJ/mol, A indicates the Arrhenius pre-exponential factor and R is 8.314 J/mol K, and (Chauhan et al., 2020, 2019; Gupta et al., 2019; Chafiq et al., 2020; Bahgat Radwan et al., 2017; Rbaa et al., 2020; Fan et al., 2019; Kikanme et al., 2020; El Kacimi et al., 2020; Ye et al., 2020; Aly et al., 2020; Tabatabaei majd et al., 2020; Dehghani et al., 2020).

The activation energy was measured from the Arrhenius plot of log $CR_{Grav.}$ versus 1000/T with the slope = E_a/2.303R. The Arrhenius plot is presented in Fig. 1(b), and the measured E_a values are given in Table 2. Overall, what stands out from the observed data shown is that the energy of activation in the inhibitor-containing medium was higher than that in the inhibitor-free system; for instance, the E_a for the metal sample was 32.84 kJ/mol, whilst it was 36.83 kJ/mol at an inhibitor concentration of 50 mg/L, confirming that the studied inhibitor increased the activation energy barrier for the electrochemical corrosion processes at the metal/electrolyte interface. It is also observed from the thermodynamic analysis that the higher E_a value is responsible for the enhanced thickness of the double layer and depends on the inhibitor concentration. Another distinguishing feature is highlighted in the investigated data: an rise in the activation energy can be responsible for the physical absorption mechanism, and the low E_a difference between the uninhibited and inhibited studied samples in the studied system indicated that the displacement between TTHIIDT molecules and pre-adsorbed-orientation water molecules on the given metal surface-solution electrolyte requires a higher E_a. This result reflects the active-energy distinction.

Continuing the thermodynamic tests, the entropy (ΔS_a) and enthalpy (ΔH_a) values of activation in the uninhibited and inhibited 1 M HCl system were derived according to Equation (4).

$$CR_{Grav.} = \frac{RT}{Nh}\exp\left(\frac{\Delta S_a}{R}\right)\exp\left(-\frac{\Delta H_a}{RT}\right) \tag{4}$$

In this transition state expressed by Equation (4), h represents the Planck constant (6.626*10^{-34} m^{2}kg/s) and N represents the Avogadro number (Chafiq et al., 2020; Bahgat Radwan et al., 2017; Rbaa et al., 2020; Tan et al., 2020a, 2020b).

The values of ΔH_a was measured by an intercept taken from the transition-state plot (log $CR_{Grav.}$/T vs. 1000/T) given in Fig. 1(c). The values of ΔH_a is presented in Table 2. In general, it is clearly evident that the positive value of ΔH_a confirmed that carbon steel dissolution is endothermic. When the TTHIIDT molecule was added to the corrosion system, the enthalpy of activation slowly increased, and this action was responsible for reducing metal dissolution. Regarding

Table 1 Dependence of temperature on the inhibition efficiency and corrosion rate at various temperatures.

C_{inh}, mg/L	Temperature, K	$CR_{Grav.}$, mg/cm^{2}hour	$\eta_{Grav.}$, %	$\theta_{Grav.}$
Blank	303	1.42	–	–
50		0.17	88.03	0.8803
100		0.1	93	0.93
150		0.012	99.15	0.9915
Blank	313	1.59	–	–
50		0.332	79.12	0.7912
100		0.264	83.4	0.834
150		0.1878	88.2	0.882
Blank	323	1.76	–	–
50		0.522	70.34	0.7034
100		0.468	73.41	0.7341
150		0.401	77.21	0.7721
Blank	333	1.93	–	–
50		0.7434	61.48	0.6148
100		0.71	63.21	0.6321
150		0.6546	66.08	0.6608

Table 2 Thermodynamic characteristics of activation for carbon steel in the inhibitor-free and the inhibitor-containing 1 M hydrochloride medium at different concentrations of the inhibitor TTHIIDT.

Parameters	No inhibitor	50 mg/L	100 mg/L	150 mg/L
E_a, kJ/mol	32.84	36.83	39.2	41.26
ΔH_a, kJ/mol	16.93	19.01	19.97	23.13
$E_a - \Delta H_a$	15.91	17.82	19.23	18.13

the difference between the activation energy and enthalpy ($E_a - \Delta H_a = RT$) values in the data shown, it was clearly noted that the TTHIIDT reactant adsorbed on the given metal surface by the effective surface area and that the rate decreased. The observed data confirmed that the studied inhibitor was characterized by unimolecular reaction behaviour and the dissolution of carbon steel and that the adsorption of this inhibitor is a unimolecular reaction according to Laidler (1963).

3.2. Electrochemical frequency modulation measurement

In the EFM analysis, the calculation of I_{crorr}, beta C and beta A depends on the corrosion mechanism types on the metal surface. Three types of corrosion mechanisms occur on the steel surface: activation, diffusion, and passive (Al-Mobarak et al., 2011; Bosch et al., 2001; Berdimurodov, 2016; Obot and Onyeachu, 2018; Abdel-Rehim et al., 2006). In this research, it was selected the activation mechanism. In the mechanism of the activated control corrosion process, the steel surface undergoes dissolution in a corrosive environment. In the steel dissolution electrochemical reaction, beta A is lower than beta C. In this type of corrosion mechanism, I_{corr}, beta C and beta A are calculated according to Equations (5)–(7) (Al-Mobarak et al., 2011; Bosch et al., 2001; Berdimurodov, 2016; Obot and Onyeachu, 2018; Abdel-Rehim et al., 2006).

$$I_{corr} = \frac{(I_{\omega_1 \cdot \omega_2})^2}{2\sqrt{8I_{\omega_1 \cdot \omega_2} I_{2\omega_2 \pm \omega_1} - 3(I_{\omega_1 \cdot \omega_2})^2}} \quad (5)$$

$$\text{Beta A} = \frac{I_{\omega_1 \cdot \omega_2} U}{I_{\omega_2 \pm \omega_1} + \sqrt{8I_{\omega_1 \cdot \omega_2} I_{2\omega_2 \pm \omega_1} - 3(I_{\omega_1 \cdot \omega_2})^2}} \quad (6)$$

$$\text{Beta C} = \frac{I_{\omega_1 \cdot \omega_2} U}{-I_{\omega_2 \pm \omega_1} + \sqrt{8I_{\omega_1 \cdot \omega_2} I_{2\omega_2 \pm \omega_1} - 3(I_{\omega_1 \cdot \omega_2})^2}} \quad (7)$$

where U is the amplitude and I is the peak currents at the different frequencies.

In the EFM experiment, two connections are important to clarify the accuracy of the EFM results. The first connection is between the response signal and the input frequency perturbation. The second connection is between the current from the intermodulation frequency and the current from the harmonic frequency. These two connections are called causality factors. In this EFM analysis, causality factors (2) and (3) were used, and they are calculated according to Equations (8) and (9); the inhibition efficiency was calculated by Equation (10), respectively (Al-Mobarak et al., 2011; Bosch et al., 2001; Berdimurodov, 2016; Obot and Onyeachu, 2018; Abdel-Rehim et al., 2006).

$$\text{Causality factor (2)} = \frac{I_{\omega_1 \pm \omega_2}}{I_{2\omega_1}} = 2 \quad (8)$$

$$\text{Causality factor (3)} = \frac{I_{2\omega_1 \pm \omega_2}}{I_{3\omega_1}} = 3 \quad (9)$$

$$\%IE_{EFM} = \frac{I^0_{corr} - I^{inh}_{corr}}{I^0_{corr}} \times 100 \quad (10)$$

where I^0_{corr} is the corrosion current in the inhibitor-free medium, I^{inh}_{corr} is the corrosion current in the inhibitor-containing medium and $\%IE_{EFM}$ is the inhibition efficiency.

The EFM intermodulation spectra for the studied material in the inhibitor-free and the inhibitor-containing 1 M hydrochloride acid solution at various concentrations of the inhibitor TTHIIDT are presented in Fig. 2. All EFM experiments were performed at 303 K. The current peaks in these intermodulation spectra correspond to the calculated corrosion current. It is clear from these spectra that the current fluctuated between approximately 125 and 170 μA for carbon steel in the inhibitor-free medium. The reason is that the 1 M HCl corrosion environment is very strong for the steel surface, and hydrogen and chloride ions affect the growth of intermodulation spectrum peaks. In contrast, the current peaks fluctuated between approximately 10 and 15 μA for carbon steel in the inhibited medium. The reason is that the inhibitor molecules affect the cathodic and anodic electrochemical half-reactions on the surface of metal, meaning that inhibitor molecules influence the surface of metal current-connection abilities and intermodulation spectrum.

The EFM analysis data for studied metal specimen in 1 M hydrochloride acid medium in the presence and absence of the inhibitor TTHIIDT at different concentrations were investigated, as presented in Table 3. The EFM experiments were performed to evaluate the activation, diffusion, and passivation corrosion mechanisms.

In the activation corrosion mechanism, the corrosion current and corrosion rates were 282.2 μA and 129 mpy, respectively, in 1 M HCl medium, which means that the carbon steel electrode dissolves in 1 M HCl medium and that Fe^{2+} and Fe^{3+} ions are formed. These ions influence the growth of the corrosion current and corrosion rates. When TTHIIDT was added to the corrosion medium, it dramatically reduced the Fe^{2+} and Fe^{3+} ion numbers by forming Fe-inhibitor complexes and adsorbing on the steel surface. Consequently, the corrosion rate and corrosion current were dramatically

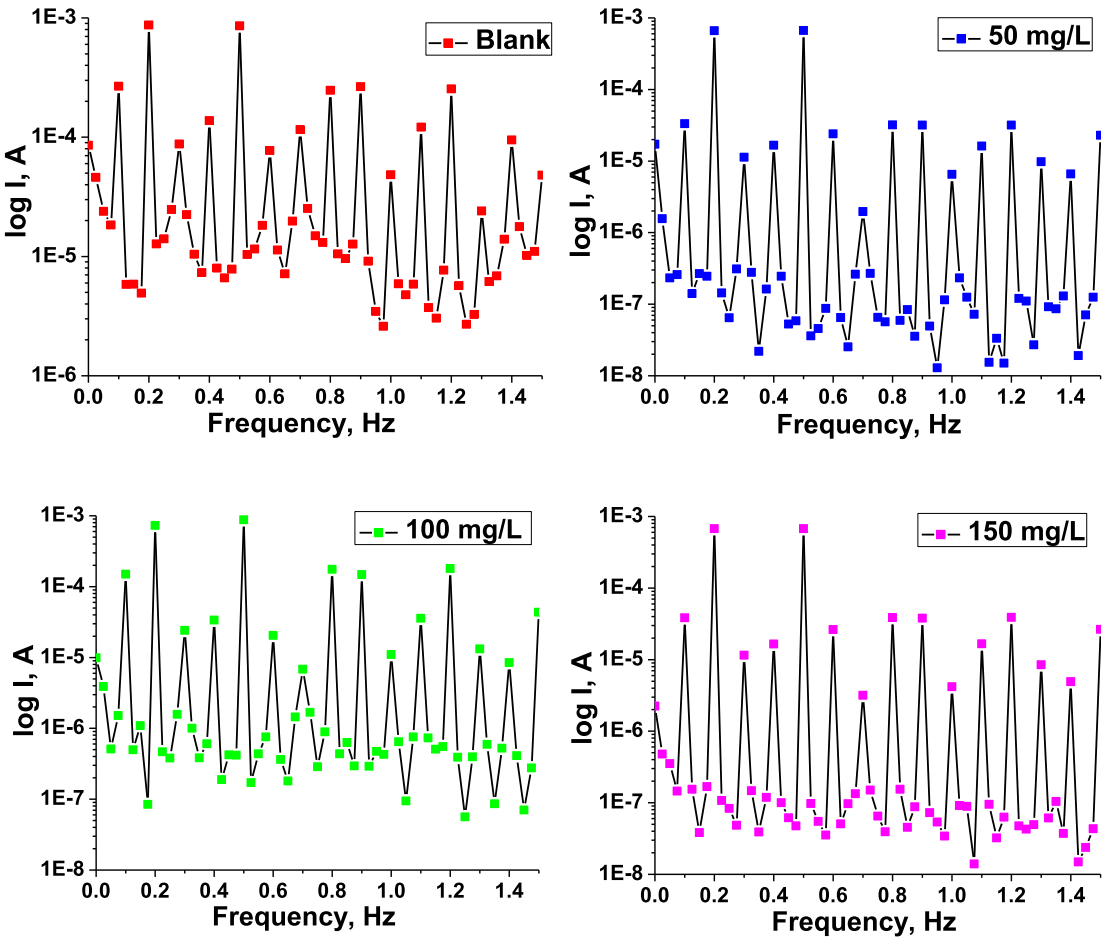

Fig. 2 EFM intermodulation spectra for carbon steel in the inhibitor-free and the inhibitor-containing 1 M HCl medium at different concentrations of the inhibitor TTHIIDT.

Table 3 EFM analysis results for carbon steel in the inhibitor-free and the inhibitor-containing 1 M HCl medium at various concentrations of the inhibitor TTHIIDT.

C_{inh}, mg/L	I_{corr}, μA	Beta A, mV/decade	Beta C, mV/decade	CR, mpy	Causa-lity factor (2)	Causa-lity factor (3)	%IE_{EFM}
Blank	282.2	19.73	23.01	129	1.95	2.96	–
50	81	81.55	105.25	37.02	1.75	2.81	71.30
100	69.19	65.87	82.21	31.63	1.93	2.95	75.48
150	51.91	54.96	78.43	23.72	2.03	3.02	81.60

reduced. This action is dependent on the inhibitor concentration.

3.3. Electrochemical noise measurements

The EN test is a highly effective and non-destructive method for corrosion investigation. The EN data are recorded based on the statistical time versus potential and current change. In the present work, EN tests for the working carbon steel electrode were carried out in 1 M HCl corrosive and inhibited medium with different amounts of the inhibitor TTHIIDT, resulting in Fig. 3, and Table 4.

In the EN analyses, the potential and current noise are derived based on Equations (11) and (12) (Danaee et al., 2019; Obot et al., 2019; Ramezanzadeh et al., 2014; Naghizade et al., 2020; Hou et al., 2016; Huet and Ngo, 2019; Ehsani et al., 2017).

$$I_{bf}[n] = A_i T[n] + B_i \tag{11}$$

$$E_{bf}[n] = A_e T[n] + B_e \tag{12}$$

where I_{bf} is the current of the standard linear best fit, E_{bf} is the potential of the standard linear best fit, A is an anodic coefficient, B is the Stern-Geary constant, T is the time at the start of the data block and n is the total point number. These equations are called the standard linear best fit equations and are used to calculate the DC trend and describe each time versus current and potential block. The electrochemical noise of the

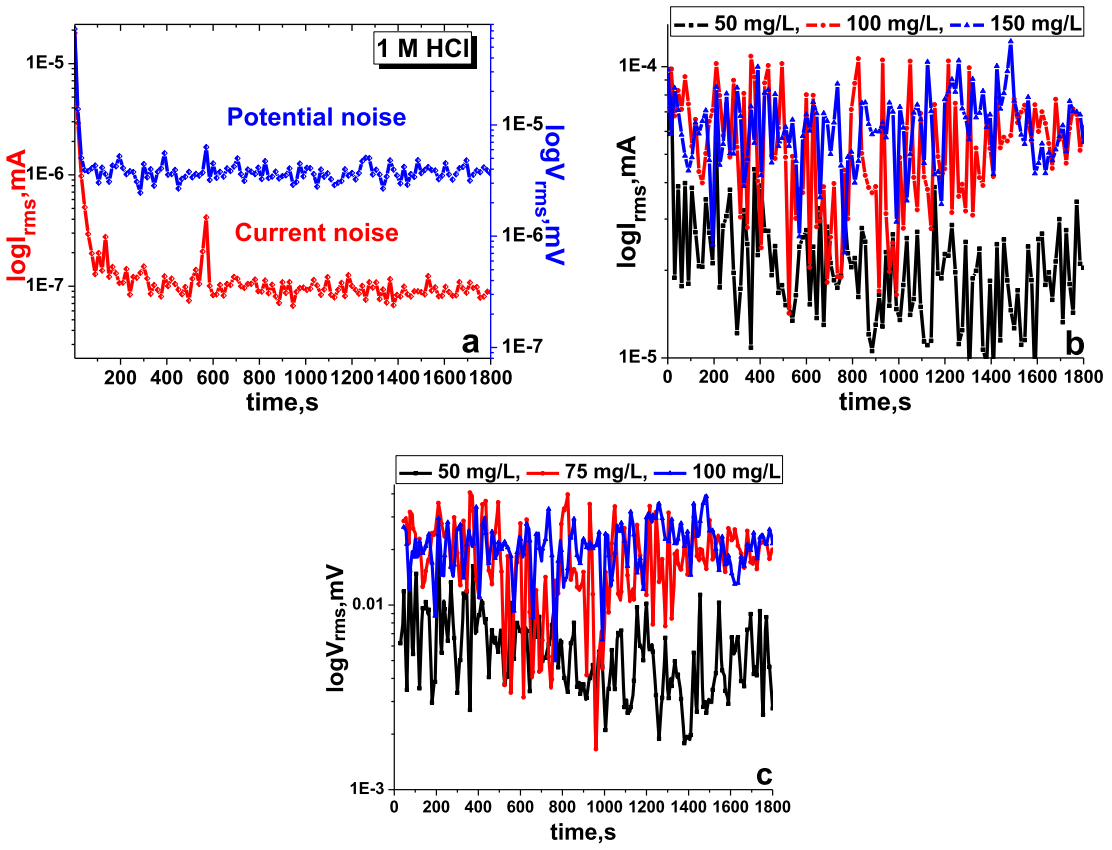

Fig. 3 Time versus current and potential noise in the inhibitor-free (a), time versus current noise (b) and potential noise (c) in the inhibitor-containing 1 M HCl medium at various concentrations of the inhibitor TTHIIDT (carbon steel).

Table 4 EN analysis results with and without various concentrations of the inhibitor TTHIIDT in 1 M HCl medium (carbon steel).

C_{inh}, mg/L	$\bar{I}_{rms}$, μA	$\bar{V}_{rms}$, μV	$\bar{R}_{rms}$, Ω	IE_{EN}, %	q, C
Blank	0.1974	4.132	20.93	–	5.6×10^{-2}
50	21.99	5983	272.08	92.30	3.9×10^{-5}
100	55.85	18,300	327.66	93.61	10×10^{-5}
150	62.99	20,920	332.11	93.70	113×10^{-5}

block is calculated by subtracting the DC trend, and it can be used to deduce the RMS (root mean square) of the residual AC signal according to Equations (13) and (14) (Danaee et al., 2019; Obot et al., 2019; Ramezanzadeh et al., 2014; Naghizade et al., 2020; Hou et al., 2016; Huet and Ngo, 2019; Ehsani et al., 2017).

$$I_{rms} = \sqrt{\frac{\sum_{n=1}^{N} \left(I[n] - I_{bf}[n]\right)^2}{N}} \tag{13}$$

$$E_{rms} = \sqrt{\frac{\sum_{n=1}^{N} \left(E[n] - E_{bf}[n]\right)^2}{N}} \tag{14}$$

In these equations, I_{rms} is the current noise, E_{rms} is the potential noise, I_{bf} is the current of the standard linear best fit, E_{bf} is the potential of standard linear best fit, N is the total channel number and n is the total point number. The current noise and potential noise can be derived from Equations (13) and (14) at given times in the EN analysis.

It is clear from Fig. 3(a) that the average potential and current noise for the working carbon steel electrode in the aggressive 1 M HCl environment fluctuated at approximately 4.132 μV and 0.1974 μA, respectively, during the time period from 1 sec to 1800 sec, indicating that the steel electrode undergoes dissolution and forms iron ions, destroying the steel electrode, which is the reason for the noise decrease. As shown in Fig. 11, these fluctuation phenomena in the potential and current noise for the studied metal electrode in the corroded environment are responsible for the metastable and nucleation processes that occur on the surface of steel. The sudden increase and decrease in the transient current and potential noise in the acid medium destroy the passive film on the steel surface.

The observed results of the time versus potential and current noise for the carbon steel electrode in the inhibitor-containing 1 M HCl medium at various concentrations of the inhibitor TTHIIDT are presented in Fig. 3(a) and (b). The electrochemical noise signals were accounted for during 1800 sec at room temperature (303 K) by EN analysis. It was shown from the observed results that the potential and current noise for the carbon steel electrode in the aggressive 1 M HCl environment slowly increased with increasing TTHIIDT concentration. The organic TTHIIDT molecules can change the electrochemical noise towards more negative values in the corrosion medium. At 50 mg/L inhibitor, the current and potential noise for steel fluctuated at approximately 21.99 μA and 5983 μV, respectively. When the inhibitor concentration was increased two-fold, the current and potential noise for steel stabilized at approximately 62.99 μA and 20920 μV, respectively. These fluctuations of noise are responsible for the active control processes occurring on the surface of carbon steel in similar metastable situations. The important increase in the current and potential noise fluctuations indicates that the organic TTHIIDT molecules are effective anti-corrosive inhibitors in aggressive acid environments.

In this EN analysis, the average current noise ($\bar{I}_{rms}$) and potential noise ($\bar{E}_{rms}$) were calculated by using the time versus average current and potential noise charts, and the measured values were applied to measure the average noise resistance ($\bar{R}_{rms}$)related to Equation (15), listed in Table 4.

$$\bar{R}_{rms} = \frac{\bar{E}_{rms}}{\bar{I}_{rms}} \tag{15}$$

Overall, Table 4 shows that the average noise resistance of the carbon steel electrode dramatically fluctuated with increasing TTHIIDT concentration in a 1 M HCl environment. This point is aptly illustrated by the fact that the $\bar{R}_{rms}$ value for the carbon steel electrode was 20.93 Ω in the corrosion medium, in contrast to the inhibited medium containing 100 mg/L TTHIIDT, whose $\bar{R}_{rms}$ value for the carbon steel electrode increased substantially to over 332.11 Ω. The reason is that the inhibitor TTHIIDT reduces the charge transfer and polarization on the surface of carbon steel electrode. The noise resistance depends on the TTHIIDT concentration and the number of inhibitor molecules, indicating that TTHIIDT forms a layer on the surface of steel and that the thickness increases with rising TTHIIDT concentration. The large layer thickness on the steel surface rapidly impacts the noise resistance, and the large noise resistance values (over 332 Ω) are responsible for the TTHIIDT organic molecules being more effective protectors for steel materials in aggressive acid corrosion environments.

In this research work, the inhibition degrees of the TTHIIDT at different concentrations in 1 M HCl solution were measured by EN analysis, and the obtained $\bar{R}_{rms}$ values were used to measure the inhibition level based on Equation (16), listed in Table 4. As observed, TTHIIDT organic molecules can protect steel electrodes from aggressive acid corrosion by over 93%, suggesting that TTHIIDT is a high-quality and valuable anti-corrosive inhibitor for steel-based materials and that it could be used in the chemical industry in order to considerably protect steel pipes and materials from corrosion.

$$IE_{EN}, \% = \frac{\bar{R}^{inh}_{rms} - \bar{R}^{0}_{rms}}{\bar{R}^{inh}_{rms}} \times 100 \tag{16}$$

where $\bar{R}^{0}_{rms}$ is the average noise resistance in inhibitor-free medium, $\bar{R}^{inh}_{rms}$ is the average noise resistance in inhibitor-containing medium and IE_{EN} is the inhibition efficiency percentage.

The inhibitor concentration versus inhibitor effectiveness in aggressive medium was measured, and the observed data are given in Table 4. As a consequence, the inhibitor TTHIIDT is a valuable protector of steel materials in terms of acid corrosion, and the protection degree depends on the inhibitor concentration.

The total charge (q) value is calculated with Gamry Echem Analyst software by using quick integration tools in the EN analysis, and the observed time is 1800 sec. In the present work, the total charge values for the working carbon steel sample were measured in the corrosion and inhibited environments, as presented in Table 4. As observed, q is 5.6×10^{-2}C for the working carbon steel sample in 1 M hydrochloride acid medium, and this q value is higher because the iron oxidation rate and the hydrogen ion reduction rate are higher, leading to the corrosion processes sharply increasing at the cathodic and anodic sites on the surface of carbon steel. The higher q value of the carbon steel electrode in the aggressive environment reflects the total cathodic and anodic electrochemical charge on the carbon steel surface, which means that the higher total charge amount is an indicator of faster charge transfer rates at the anodic and cathodic sites of the carbon steel surface and that strong corrosion processes occur.

The variation in the total charge versus TTHIIDT concentration in 1 M HCl was investigated, and the results are given in Table 4. When the inhibitor TTHIIDT was added to the corrosion environment, the total charge value significantly decreased by nearly three-fold, and this change depended on the TTHIIDT concentration. At higher concentrations of the inhibitor TTHIIDT (100 mg/l), the q value is 113×10^{-5} C, which is three-fold greater than that for the uninhibited environment, suggesting that the TTHIIDT molecules considerably decreased the iron oxidation rate and hydrogen evolution at the anodic and cathodic sites of the surface of carbon steel in 1 M HCl medium. The next indicator for q reduction is the adsorption of TTHIIDT on the surface of steel because these inhibitor molecules maximally blocked charge transfer from the anodic sites to cathodic sites.

3.4. Open-circuit potential

Open-circuit potential changes were investigated in 10 min for carbon steel in 1 M depassivator solution with various concentrations of inhibitor at 313 K, as shown in Fig. 4(a). It is clear from these results that the OCP remained stable in all experiments, suggesting that metal oxides, hydroxides and other adsorbed compounds dissolve on the surface of metal and that the inhibitor adsorbs on the surface of metal. The OCP curves in inhibitor-free 1 M HCl medium were stable at approximately −0.435 mV. When inhibitor was added to this aggressive medium, the OCP shifted to more negative values (cathodic site). This change depends on the inhibitor concentration: at 50 mg/l, it is −0.542 mV; at 100 mg/l, it is −0.543 mV; and at 150 mg/l, it is −0.559 mV. The OCP time

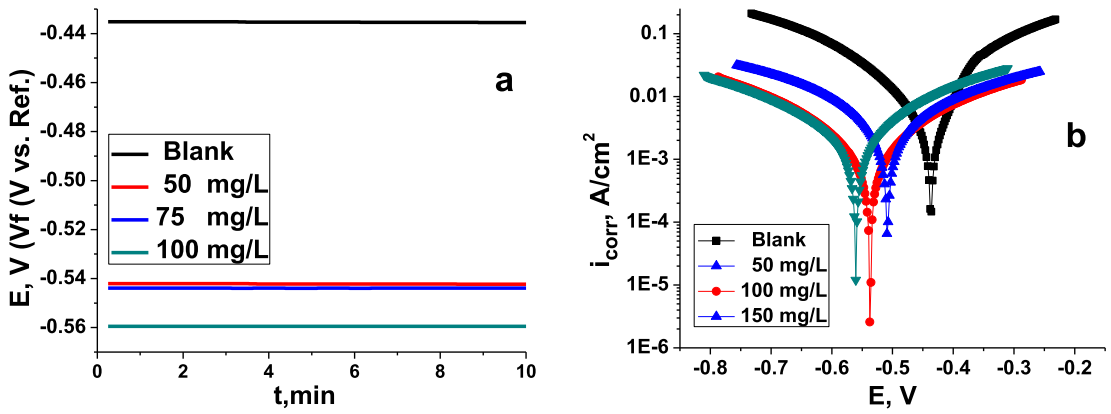

Fig. 4 The change in OCP (a) and Tafel curves (b) for carbon steel in the inhibitor-free and the inhibitor-containing 1 M depassivator solution at different concentrations of the inhibitor TTHIIDT (313 K).

curves remained stable around the negative potential, which suggests that the inhibitor formed passive films on the steel surface. As observed, the equilibrium potential (OCP) shifts to more negative potentials. The reason why the shift towards negative potentials is due to the structure of the inhibitor molecules and the orientation (Fig. 10) on the electrode surface. The inhibitor consists of lone paired electrons due to the presence of nitrogen and sulfur atoms (Fig. 10) and the benzene rings, which are rich in electrons and hence are more negatively charged at the electrode surface. Thus the potential shifts towards negative direction with the presence of the inhibitor.

3.5. Potentiodynamic polarization measurements

To examine the electrochemical kinetics of the cathodic and anodic corrosion activities on the surface of carbon steel in the inhibitor-free and the inhibitor-containing 1 M HCl medium at different concentrations of the inhibitor TTHIIDT, the PDP cathodic and anodic curves were investigated, and the observed data are given in Fig. 4(b). As observed, the cathodic and anodic Tafel curves for metal specimen noted on more positive and higher current density areas in 1 M HCl medium indicate that H^+ and Cl^- ions promote the anodic and cathodic electrochemical half-reactions on the surface of metal as a result of aggressive destruction of the carbon steel electrode surface (Chauhan et al., 2019; Gupta et al., 2019; Chafiq et al., 2020; Bahgat Radwan et al., 2017; Rbaa et al., 2020; Tan et al., 2020a, 2020b).

It can also be shown in Fig. 4(b) that the organic inhibitor TTHIIDT shifted both the electrochemical cathodic and anodic Tafel curves to lower current density and more negative potentials areas, indicating that the TTHIIDT molecules dramatically diminished both anodic and cathodic electrochemical half-reactions that cause corrosion of the steel surface. The observed Tafel curves suggest that the TTHIIDT organic molecule is a mixed-type inhibitor and that its anti-corrosion activities depend on the concentration.

The observed Tafel curves were shifted to more negative potentials with rising inhibitor concentration because the adsorption degree of TTHIIDT molecules depends on the concentration; therefore, a higher inhibitor concentration is responsible for more adsorption, and the many inhibitor molecules occupy a wide area of the surface of carbon steel. As a result, the adsorbed inhibitor molecules significantly decreases the number of electrochemical cathodic and anodic corrosion active sites on the surface of metal working electrode.

The electrochemical potentiodynamic polarization Tafel characteristics of the studied working electrode, called the corrosion current density (i_{corr}), corrosion potential (E_{corr}), corrosion rate (CR_{PDP}), inhibition efficiency (η_{PDP}), corrosion resistance (R_{PDP}), surface coverage degree (θ_{PDP}), Stern-Geary constant (B), corrosion resistance (R_{PDP}), Tafel anodic beta (Beta A) and cathodic beta (-Beta C) slopes, were measured from Fig. 4(b) through Tafel extrapolation analysis, summarized in Table 5.

As investigated, the corrosion density was recorded as 71.2 mA/cm^2 in HCl medium without an inhibitor because a higher number of H^+ and Cl^- ions is the main cause for an increased corrosion current at the carbon steel surface. In comparison with that of the inhibited medium, the corrosion density sharply decreased to 7.64 mA/cm^2 at 50 mg/L TTHIIDT, 3.63 mA/cm^2 at 100 mg/L and 1.25 mA/cm^2 at 150 mg/L, confirming that the organic inhibitor TTHIIDT maximally neutralized H^+ and Cl^- ions on the carbon steel electrode. These decreases in the corrosion current density depend on the TTHIIDT concentration, which means that a higher concentration is responsible for a greater reduction in metal destruction.

In PDP analysis, the organic inhibitors are classified (cathodic, anodic and mixed types) according to the difference in potential between uninhibited and inhibited environments, meaning that for a value below 85 mV, potential displacement indicates that the studied inhibitor behaviour is mixed, which impacts both anodic and cathodic electrochemical reactions on the surface of metal electrode, while for a potential difference above 85 mV, an inhibitor may be categorized as cathodic or anodic. The obtained PDP measurements show that the potential displacement was 71 mV at 50 mg/L TTHIIDT; this phenomenon confirmed that the behaviour of the inhibitor TTHIIDT is mixed at this concentration, indicating that TTHIIDT molecules effectively influence both cathodic and anodic electrochemical corrosion reactions.

It can also be observed in Table 5 that the potential difference reported was 100 mV at 100 mg/L and 123 mV at 150 mg/L, suggesting that the inhibitor TTHIIDT is categorized as anodic. The reason is that TTHIIDT more influences electro-

Table 5 Electrochemical potentiodynamic polarization Tafel properties for carbon steel in the inhibitor-free and the inhibitor-containing 1 M HCl medium at various concentrations of the inhibitor TTHIIDT (313 K).

Parameters	C_{inh}, mg/L			
	Blank	50	100	150
i_{corr}, mA/cm^2	71.2	7.64	3.63	1.25
E_{corr}, mV	−437	−508	−537	−560
Beta A, mV/decade	135.4	112.5	105.9	98.4
Beta C, mV/decade	185.7	155.2	135.6	120.1
CR_{PDP}, mpy	90.43	3.489	1.657	0.572
η_{PDP}, %	–	89.26	94.9	98.24
θ_{PDP}	–	0.8926	0.949	0.9824
B_{PDP}, mV	34	28.32	25.81	23.48
R_{PDP}, Ω/cm^2	0.47	3.7	7.11	18.78

chemical anodic corrosion processes by neutralized Fe^{2+} ions at the cathodic sites of the surface of carbon steel. It is notable from the results that the Tafel anodic beta (Beta A) and cathodic beta (-Beta C) slopes for carbon steel were 135.4 and 185.7 mV/decade, respectively, in the aggressive acid medium; in inhibited medium, the inhibitor TTHIIDT substantially changed these values to more negative and positive potential sites. This phenomenon confirmed that TTHIIDT effectively impacts the cathodic and anodic corrosion on the carbon steel surface as a consequence the massive reduction in hydrogen evolution and steel dissolution.

It was clearly indicated that CR_{PDP} is very fast in 1 M HCl medium, at 90.43 mpy, but it dramatically decreased to 0.572 mpy with 100 mg/L TTHIIDT added to the corrosion medium. In view of the fact that TTHIIDT molecules are adsorbed via a flat orientation and cover wide areas on the surface of carbon steel electrode, as the amount of TTHIIDT increases, its molecules are perpendicularly adsorbed on the surface of carbon steel electrode because this inhibitor is water-soluble and highly polarized. An rise in the number of TTHIIDT molecules is responsible for increased electrostatic repulsion and forces between these inhibitor molecules.

In the present research work, the inhibition efficiency (η_{PDP}) and surface coverage scale (θ_{PDP}) were derived according to Equations (18) and (19), respectively.

$$\eta_{PDP},\% = \frac{i^{o}_{PDP} - i^{i}_{PDP}}{i^{o}_{PDP}} \times 100\% \tag{18}$$

where i^{o}_{PDP} is the corrosion current density in the aggressive acid medium, i^{i}_{PDP} is the corrosion current density in the inhibited medium and $\eta_{PDP}$is the inhibition efficiency.

$$\theta_{PDP} = \frac{\eta_{PDP}}{100} \tag{19}$$

where θ_{PDP} is the surface coverage scale and η_{PDP} is the inhibition efficiency.

The η_{PDP} of the inhibitor TTHIIDT was over 90%, confirming that this investigated inhibitor is a more effective corrosion protector for carbon steel in an aggressive hydrochloride environment. It is also said that this phenomenon depends on the TTHIIDT concentration. Another distinguishing feature in Table 5 is that the inhibitor TTHIIDT maximally covered the area on the carbon steel surface by adsorption.

In the PDP examination, the Stern-Geary constant (B) was measured related to Equation (20), and the impact of the amount of TTHIIDT on the Stern-Geary constant was tested, as listed in Table 5. According to the data shown, the measured B value for the carbon steel electrode in 1 M HCl medium was 34 mV. By adding 50 mg/L TTHIIDT to the HCl environment, B noticeably decreased to 28.32 mV. This drop depends on the inhibitor TTHIIDT concentration, and when the concentration was increased two-fold, the value B significantly decreased to 23.48 mV.

$$B_{PDP} = \frac{\text{Beta A} \times \text{Beta C}}{2.303(\text{Beta A} + \text{Beta C})} \tag{20}$$

where BetaA is the Tafel anodic beta, Beta C is the Tafel cathodic beta, and B_{PDP} is the constant of Stern-Geary.

The corrosion resistance of the studied metal electrode in a 1 M HCl environment without and with the inhibitor TTHIIDT were deduced by using Equation (21), as indicated in Table 5.

$$R_{PDP} = \frac{B_{PDP}}{i_{PDP}} \tag{21}$$

where B_{PDP} is the Stern-Geary constant, R_{PDP} is the corrosion resistance and i_{PDP} is the corrosion current density.

Generally, the carbon steel electrode has a low resistance to corrosion attack, which was reported to be 0.47 Ω/cm^2. However, 100 mg/L TTHIIDT dramatically increased this corrosion resistance to 18.78 Ω/cm^2, indicating that the inhibitor TTHIIDT adsorbed on the carbon steel electrode and effectively resisted both cathodic and anodic corrosion activities.

3.6. Electrochemical impedance spectroscopy measurements

All EIS data were obtained by using the Levenberg-Marquardt method on the equivalent circuit model, which is represented in Fig. 5. This approach used an equivalent circuit model containing the CPE (constant phase element), R_s (solution resistance) and R_{ct} (charge transfer resistance). The constant phase element has been used for the capacitor with the aim of investigating accurate fitting of the circuit; it can be expressed according to Equation (22).

$$Z_{CPE} = Y_0^{-1}(i\omega)^{-n} \tag{22}$$

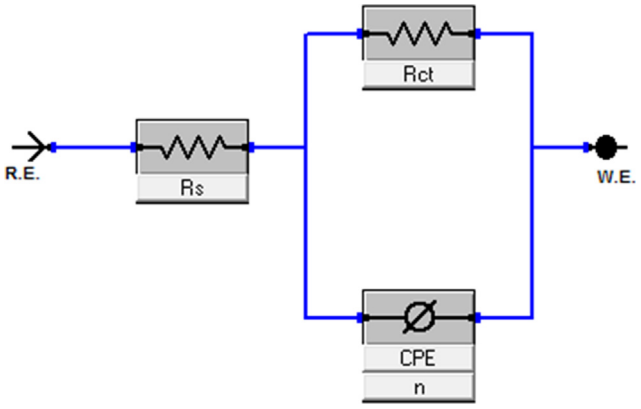

Fig. 5 An equivalent circuit model was utilized to calculate the EIS parameters.

In this equation, ω is an angular frequency, Y_0 and i are the constant phase element magnitude and an imaginary number, respectively, and n is the empirical constant, which is less than one and responsible for calculating the heterogeneity of the carbon steel-electrolyte interface (Chauhan et al., 2020, 2019; Gupta et al., 2019; Chafiq et al., 2020; Bahgat Radwan et al., 2017; Rbaa et al., 2020; Tan et al., 2020; Fan et al., 2019; Kikanme et al., 2020; El Kacimi et al., 2020; Ye et al., 2020).

The level of double-layer capacitance was derived from the constant phase element value and is given by Equation (23).

$$C_{dl} = \left(Y_0 R_{ct}^{1-n}\right)^{1/n} \tag{23}$$

where R_{ct} is the polarization resistance and C_{dl} is the double-layer capacitance level.

As indicated by the measured C_{dl} in Table 6, the level of C_{dl} in the inhibited aggressive acid medium was nearly five-fold lower than that in the uninhibited aggressive acid medium (298.16 $\mu F/cm^2$), demonstrating that the inhibitor TTHIIDT decreased the local dielectric constant in 1 M hydrochloride acid solution and increased the double layer's thickness, which is illustrated related to the Helmholtz model (Equation (24)) (Fan et al., 2019; Kikanme et al., 2020; El Kacimi et al., 2020; Ye et al., 2020; Aly et al., 2020; Tabatabaei majd et al., 2020; Dehghani et al., 2020; Lgaz et al., 2020).

$$C_{dl} = \frac{\varepsilon\varepsilon^0}{d} A \tag{24}$$

where ε and ε^0 are the dielectric constants of vacuum and the corresponding environment, respectively, and d is the double layer's thickness the on the surface of carbon steel.

The kinetic characteristics of the carbon steel/electrolyte interface processes and surface properties were investigated by the EIS method. The Nyquist plots for carbon steel in the inhibitor-free and the inhibitor-containing 1 M HCl medium at different concentrations of the inhibitor TTHIIDT are depicted in Fig. 6(a). As observed, the obtained plots for the carbon steel/electrolyte interface in the investigated hydrochloride acid environment with and without different values of TTHIIDT organic inhibitor were single depressed capacity semicircles, indicating that the corrosion processes on the surface of carbon steel are dominated by a charge transfer mechanism. It can also be seen from the obtained results that the Nyquist plots in the 1 M HCl solution are very small depressed semicircles, confirming that the corrosion activities are faster at the carbon steel surface-electrolyte interface. In the inhibited 1 M HCl solution, TTHIIDT dramatically diminished all electrochemical corrosion reactions by controlling the charge transfer mechanism at the carbon steel-electrolyte interface. It should be sensible to emphasize that the size of the Nyquist semicircle increases with the amount of TTHIIDT. This trend is responsible for the inhibitor TTHIIDT forming a protective layer and adsorbing at the carbon steel-electrolyte interface. Another outstanding point from Fig. 6(a) is that the obtained depressed capacity semicircles were cited at upper frequencies, indicating that the corrosion activities controlled by charge transfer and the double-layer capacity are lower in HCl acid solution, while the obtained small depressed inductive semicircles were located at lower frequencies, indicating that the relaxation TTHIIDT occurred at carbon steel-electrolyte interface (Chauhan et al., 2020, 2019; Gupta et al., 2019; Chafiq et al., 2020; Bahgat Radwan et al., 2017; Rbaa et al., 2020; Tan et al., 2020a, 2020b).

As illustrated in Table 6, the polarization resistance value was 4.599 Ω/cm^2 in 1 M HCl solution, and this value sharply increased to over 30 Ω/cm^2 in inhibited 1 M HCl solution. The R_{ct} value rose with increasing TTHIIDT concentration, which is responsible for forming a thick protective film the surface of carbon steel. This phenomenon confirmed that the corrosion activities on the surface of carbon steel are controlled by polarization resistance, which is a complex resistance and comprises five types of resistance: diffusion layer resistance (R_{dl}), charge transfer resistance (R_{ct}), protective layer resistance (R_{pl}), and accumulation resistance (R_a) and solution resistance (R_s). The charge transfer resistance illustrates the displacement into the real impedance between the maximum and minimum frequencies.

The second notable feature is that the double-layer capacitance remarkably decreased in the inhibited hydrochloride environment. This phenomenon is responsible for the TTHIIDT molecules adsorbed on the surface of carbon steel as well as the reduced electrical conductivity through the substitution of TTHIIDT molecules with orientation-adsorbed water molecules on the surface of carbon steel. As shown in Table 6, the n value in the uninhabited medium was greater than that in the inhibited medium, indicating that the aggressive hydrochloride solution made the carbon steel surface more homogenous. According to the data shown, the R_s value was 1.420 Ω/cm^2 in 1 M hydrochloride solution, which is attributed to the higher solution conductivity. However, the inhibitor TTHIIDT sharply decreased the solution conductivity by decreasing R_s to 4.383 Ω/cm^2. As Table 6 shows, the R_{ct} value rapidly increased with the addition of TTHIIDT to 1 M hydrochloride solution compared to that without TTHIIDT, suggesting that the inhibitor effectively blocked both the cathodic and anodic active sites on the surface of carbon steel. In the present research, the inhibition efficiency degree was measured by using the obtained R_{ct} value, based on Equation (25).

$$\eta_{EIS}, \% = \frac{R_{ct}^i - R_{ct}^o}{R_{ct}^i} \times 100\% \tag{25}$$

where R_{ct}^i and R_{ct}^o are the resistance values of charge transfer for carbon steel in the inhibitor-free and the inhibitor-

Table 6 EIS data for carbon steel in the inhibitor-free and the inhibitor-containing 1 M HCl medium at different concentrations of the inhibitor TTHIIDT.

C_{inh}, mg/L	R_s, Ω/cm^2	$Y_0 \times 10^{-3}$, S-s^n/cm^2	n	R_{ct}, Ω/cm^2	η_{EIS}, %	C_{dl}, μF/cm^2	The goodness of Fit $\times 10^{-6}$
Blank	1.420	48.93	0.7522	4.599	–	298.16	35.59
50	3.771	1.464	0.8305	30.38	84.8	52.55	36.35
100	4.048	1.263	0.8456	35.93	87.2	52.66	33.48
150	4.383	1.144	0.8707	42.99	89.3	55.48	26.76

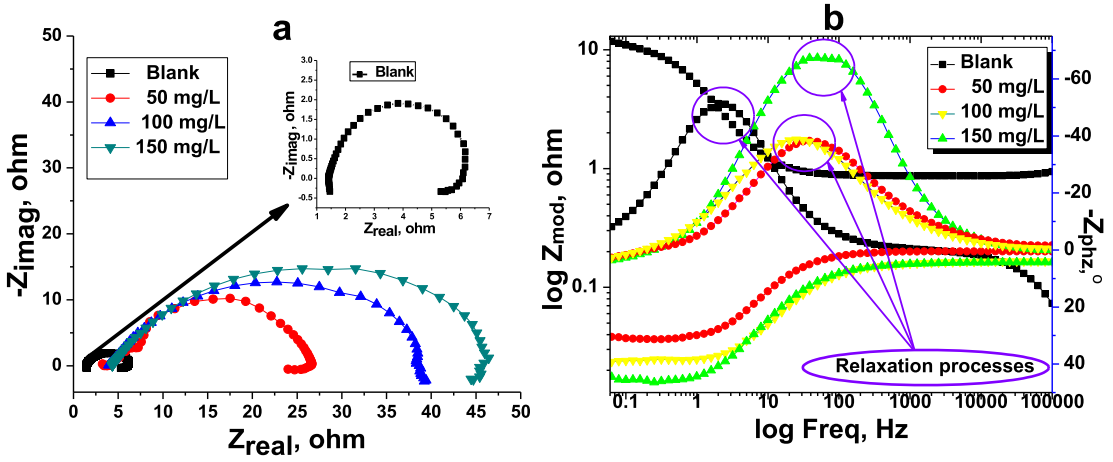

Fig. 6 Nyquist (a), phase angle and Bode (b) plots for carbon steel in the inhibitor-free and the inhibitor-containing 1 M HCl medium at different concentrations of the inhibitor TTHIIDT.

containing 1 M HCl medium at different concentrations of the inhibitor TTHIIDT, respectively, and η_{EIS} is the inhibition efficiency degree.

As shown in Table 6, the inhibition efficiency of the inhibitor TTHIIDT generally was over 85% and depended on the inhibitor concentration. These results confirmed that the investigated inhibitor was an effective protector of carbon steel in an aggressive acid environment. In this research paper, the goodness of fit for the EIS test was measured according to the Kronig-Kramers transform, as given in Table 6. It is remarkable that the goodness of fit for the EIS test was lower than 1×10^{-5}, confirming that the observed EIS data were more accurately derived by the studied impedance spectra and used the equivalent circuit model.

The phase angle and Bode plots for the carbon steel in the inhibitor-free and the inhibitor-containing 1 M HCl medium at different concentrations of the inhibitor TTHIIDT are shown in Fig. 6(b) and Table 7. The n factor was calculated according to the given Bode and phase angle diagrams, and its value is equal to the difference of the ideal capacitance characteristics. The obtained results support that the inhibitor TTHIIDT improved the surface roughness of carbon steel. As indicated in Fig. 6(b), the phase angle decreased with increasing TTHIIDT concentration, and the minimum Z_{phz} was −68.48° at 100 mg/L TTHIIDT. In EIS theory, it was demonstrated that the phase angle is −90° and the constant slope is −1. In the present work, it was found that the minimum phase angle and the slopes were −68.48° and 0.637, respectively, revealing that the carbon steel-electrolyte interface exhibited non-ideal capacitance behaviour and that its capacitance characteristics were at intermediate frequencies. This intermediate frequency of the Bode-phase angle diagram included a single uppermost trend with one stabilization time. This phenomenon suggests that the single relaxation activities (circled in Fig. 6(b)) occurred during the charge transfer process on the steel surface in both uninhibited and inhibited hydrochloride environments.

The extent of deviation from the ideal capacitor characteristics is attributed to the surface smoothness of the surface of the carbon steel-solution interface. It can be inferred that the measured differences from ideal capacitance characteristics were responsible for the carbon steel surface smoothness. The difference in the phase angle and slope relative depends on an increase in the TTHIIDT concentration and is responsible for the decreasing trend of the corrosion rate and carbon steel dissolution in the acid solution.

3.7. Adsorption isotherm

In this current research, the Langmuir isotherm was utilized to identify the adsorption behaviour of the studied inhibitor, as reflected in Equation (26) (Chauhan et al., 2019; Gupta et al., 2019; Chafiq et al., 2020; Bahgat Radwan et al., 2017; Rbaa et al., 2020; Tan et al., 2020a, 2020b).

$$\frac{C_{inh}}{\theta_{Grav.}} = \frac{1}{K_{ads}} + C_{inh} \tag{26}$$

where $\theta_{Grav.}$ signifies the surface coverage degree and K_{ads} indicates the equilibrium constant of the adsorption–desorption processes of inhibition.

Table 7 The minimum and maximum characteristics were measured from the phase angle plots for carbon steel in the inhibitor-free and the inhibitor-containing 1 M HCl medium at different concentrations of the inhibitor TTHIIDT.

C_{inh}, mg/L	Z_{mod}, Ω		Freq, Hz		Z_{phz}, °	
	min	max	min, kHz	max, mHz	min	max
Blank	1.411	6.203	3.993	63.14	−22.33	18.76
50	3.540	31.31	25.14	178.5	−36.51	2.698
100	3.962	39.48	56.24	230.1	−38.28	3.424
150	4.338	46.45	79.51	251.5	−68.48	3.995

The obtained Langmuir isotherm is given in Fig. 7(a) and indicates $C_{inh}/\theta_{Grav.}$ vs. $\theta_{Grav.}$ plots related to various temperatures. The intercepts from these plots were utilized to calculate K_{ads} and the regression coefficient (R^2), and the results are noted in Table 8. It should be emphasized that the obtained Langmuir isotherms illustrated the adsorption behaviour of the investigated inhibitor, forecasting the equivalent of $\theta_{Grav.}$ in active sites and the homogeneity of the studied surface. The most striking feature that the R^2 values were near 1 at all concentrations, and the obtained slopes from the Langmuir plots were a unity. This phenomenon illustrated that the inhibitor TTHIIDT formed a single thick layer on the surface of carbon steel.

In the next part of the adsorption analysis, the calculated K_{ads} values were used to measure the change in standard free energy (ΔG^o_{ads}) related to Equation (27), with the values presented in Table 8.

$$\Delta G^o_{ads} = -RTln(1000K_{ads}) \quad (27)$$

where the concentration of water in a given system is 1000 L/g (Chauhan et al., 2020, 2019; Gupta et al., 2019; Chafiq et al., 2020; Bahgat Radwan et al., 2017; Rbaa et al., 2020; Tan et al., 2020a, 2020b).

In the adsorption processes, the changes in the standard enthalpy (ΔH^o_{ads}) and entropy (ΔS^o_{ads}) values were responsible for signifying the adsorption type and the molecular interaction behaviour of the studied inhibitor on the surface of carbon steel. The values ΔH^o_{ads} and ΔS^o_{ads} were deduced according to Equation (28) (Gupta et al., 2019; Chafiq et al., 2020; Bahgat Radwan et al., 2017; Rbaa et al., 2020; Tan et al., 2020a, 2020b; Fan et al., 2019; Kikanme et al., 2020; El Kacimi et al., 2020; Ye et al., 2020; Aly et al., 2020); and their values are indicated in Table 8.

$$\Delta G^o_{ads} = \Delta H^o_{ads} - T\Delta S^o_{ads} \quad (28)$$

As seen from Table 8, the higher adsorption–desorption constant is responsible for effective adsorption of the inhibitor TTHIIDT on the surface of carbon steel. Another significant point from the data is that the obtained change in ΔG^o_{ads} behaviour of the studied inhibitor depends on the physical and chemical interaction mechanisms between the surface and inhibitor. The negative change in the standard Gibbs energy confirmed that this interaction mechanism involves spontaneous adsorption. ΔG^o_{ads} is a function of temperature change, as represented in Fig. 7(b), which indicates the adsorption characteristics of TTHIIDT. According to corrosion science research, an amount of ΔG^o_{ads} below −20 kJ/mol, representing the physical adsorption mechanism, involves electrostatic interactions between the surface and inhibitor, whilst an amount above 40 kJ/mol of ΔG^o_{ads} reflects chemical adsorption, which is carried out by the formation of chemical bonds. As investigated, the ΔG^o_{ads} value was between −23 and −25 kJ/mol. This result confirmed that the adsorption of TTHIIDT on the surface of carbon steel involves physisorption and chemisorption processes and suggests that physical adsorption is more dominant than chemical adsorption with rising temperature. Remarkably, from the observed data, the change in the standard enthalpy for TTHIIDT was −2.34 kJ/mol, which confirmed that the adsorption action of this inhibitor on the carbon steel surface is endothermic. Moreover, the change in standard

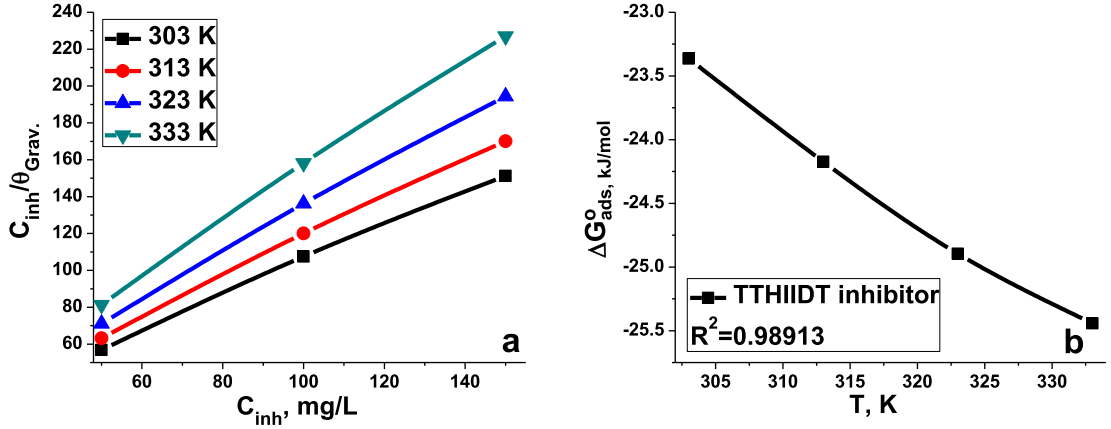

Fig. 7 Langmuir isotherm plots (a) and the relationship between ΔG^o_{ads} and temperature (b) for carbon steel in the inhibitor-free and the inhibitor-containing 1 M HCl medium at different concentrations of the inhibitor TTHIIDT.

Table 8 The thermodynamic parameters for carbon steel in the inhibitor-free and the inhibitor-containing 1 M HCl medium at various concentrations of the inhibitor TTHIIDT.

Temperature, K	K_{ads}, g/L	R^2	ΔG^o_{ads}, kJ/mol	ΔH^o_{ads}, J/mol	ΔS^o_{ads}, J/mol
303	10.71	0.9964	−23.364	−2.34	−70
313	10.87	0.9974	−24.173		
323	10.67	0.9978	24.895		
333	9.84	0.998	−25.442		

entropy was −70 J/mol, and this lower value suggested that the adsorption of this inhibitor is promoted by reducing the disorder on the steel surface.

On the other hand, it is obviously indicated that the activation entropy values were lower in the TTHIIDT-containing system than in the inhibitor-free system, suggesting that the disorder in the studied system was reduced by forming the adsorbing active metal-inhibitor complexes and the displacement between the inhibitor and pre-adsorbed water molecules.

3.8. Surface measurements

SEM images of the carbon steel surface in in the inhibitor-free and the inhibitor-containing 1 M HCl medium at the optimum concentrations of the inhibitor TTHIIDT were obtained after 3 h of immersion, as displayed in Fig. 8. It is clear from Fig. 8 (a) that the surface of carbon steel was seriously destroyed and corroded in the studied uninhibited environment through an aggressive attack by H^+ and Cl^- ions. It was shown, from the observed SEM images of the carbon steel surface in the TTHIIDT-containing solution, the surface morphology damage was dramatically diminished (Fig. 8(b)). This phenomenon occurred through the formation of a thin protective layer on the surface of carbon steel. Overall, what stands out from the data is that the obtained SEM micrographs confirmed that the inhibitor TTHIIDT effectively insulated the carbon steel surface from aggressive corrosion attack and importantly reduced corrosion processes by its high adsorption capacitance.

3.9. Quantum chemical calculations

3.9.1. Optimization analysis

The DFT-based quantum chemical measurements could give valuable opportunities to predict the global reactivity indicator value of the investigated inhibitor. The B3LYP method was performed in the DFT calculations with 6-311G (d, p) basis sets. Before starting DFT analysis, the observed inhibitor molecule was optimized, and the resulting optimized molecular structure is presented in Fig. 9(a). As illustrated, it was computed that the studied inhibitor molecule was the comparatively largest planar structure molecule. It is noticeable that three planar rings (two benzoyl rings and one hetero ring) were present in the TTHIIDT molecule, indicating that these planar groups can promote the functioning of this inhibitor as a good adsorbent on the surface of carbon steel. Additionally, the broad stretched and larger planar linked atoms in this inhibitor molecule could promote effective intermolecular interactions between the surface of the carbon steel-electrolyte interface and the researched inhibitor molecule.

3.9.1.1. Frontier molecular orbital electron density distribution analysis. The energies of highest occupied molecular orbital (HOMO) and the lowest unoccupied molecular orbital (LUMO) of the inhibitor TTHIIDT were computed and utilized to estimate the different types of global reactivity property values of the studied inhibitor through frontier molecular orbital (FMO) analysis. The corrosion inhibition characteristics of the inhibitor TTHIIDT were anticipated according to the FMO-based computed reactivity behaviours.

The LUMO and HOMO electron density distribution energies of the observed inhibitor were computed by DFT-FMO quantum calculation analysis, as depicted in Fig. 9(c and d). From the computed HOMO and LUMO, it is an outstanding indicator that the HOMO and LUMO regions in the investigated inhibitor molecule are responsible for the electron donor and acceptor behaviour of this inhibitor, respectively. It could also be highlighted from the observed FMO orbitals that the HOMO and LUMO sites in the TTHIIDT molecule reflected the active regions that are putatively responsible for electron transport from the inhibitor to the surface of carbon steel. As observed from Fig. 9(c), the HOMO electron density distribution is mainly located around sulfur atoms, illustrating that the electron donation processes to free vacancy d-orbitals of iron are mainly supported by sulfur atoms in the studied inhibitor molecule. In contrast, in Fig. 9(d), the LUMO mainly has a density around phenyl rings, indicating that the phenyl rings are responsible for the acceptor tendency of the studied inhibitor. The obtained molecular electrostatic potential (MEP) (Fig. 9(b)) indicated the reactive sites of optimised structure. MEP is also responsible for the active sites of nucleophilic and electrophilic attack. In the obtained MEP, while blue (positive) regions are responsible for the electrophilic reactivity and the red (negative) regions are responsible for nucleophilic attack.

3.9.2. Atomic charge distribution analysis

The atomic charge distribution can also illustrate molecular reactivity descriptors and active sites of organic molecules. In this research work, the charge distribution was computed, resulting in Fig. 10. Overall, what stands out from the observed charge distribution is that nearly 90% of atoms in the studied inhibitor were more negatively charged, which indicates improved adsorption capacitance of this organic inhibitor. It is a remarkable feature from the observed results that the atoms 2 N, 4 N, 5 N, 6 N, 8S, 10S, 23C and 24C were more negative in a given structure, so they promote better electron-donor tendency and chemical adsorption abilities of the studied inhibitor. In contrast, atoms 7C and 9C were more positively charged than other atoms, which supports the effective electron-acceptor capacitance and physical adsorption

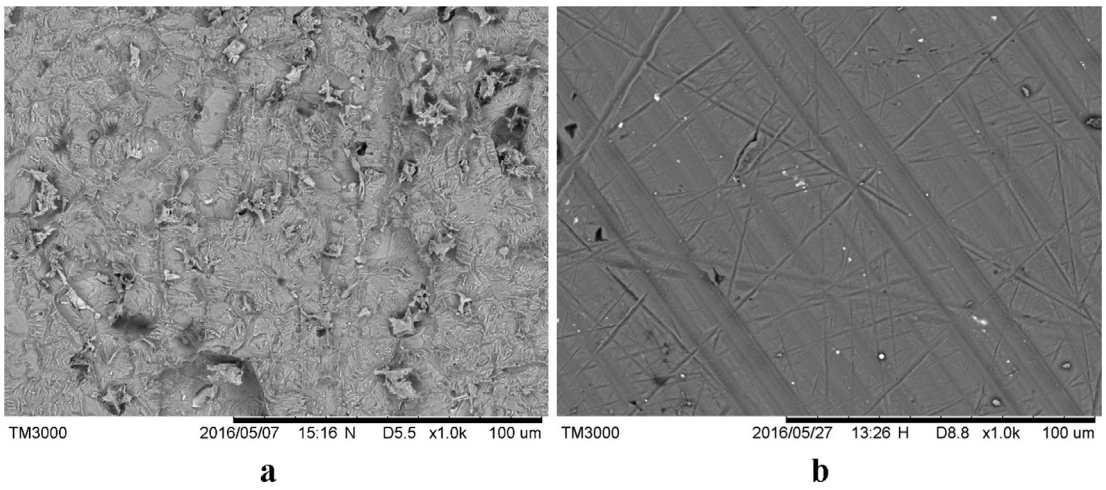

Fig. 8 SEM micrographs for carbon steel in the inhibitor-free (a) and the inhibitor-containing (b) 1 M HCl medium at the optimum concentrations of the inhibitor TTHIIDT.

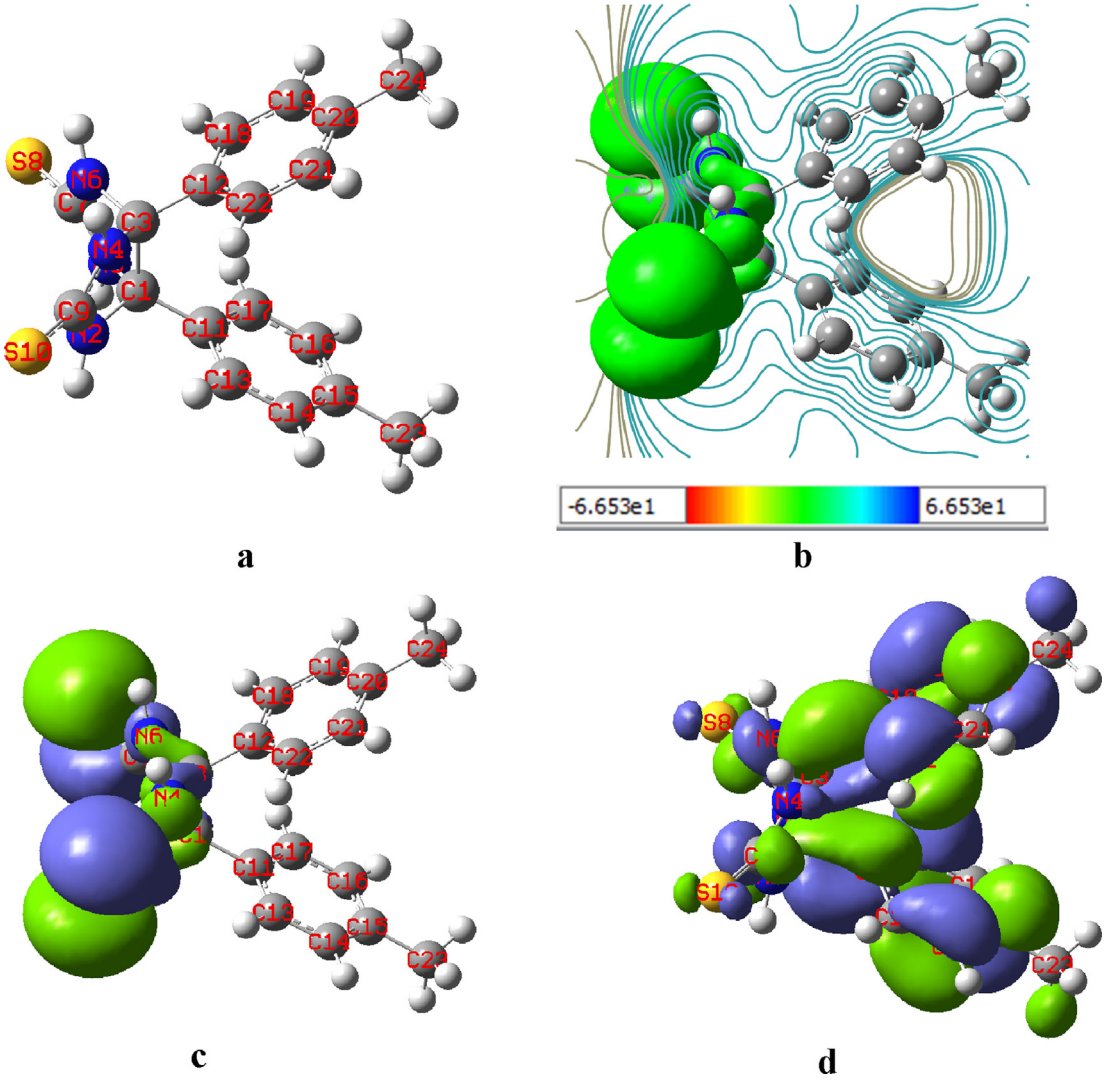

Fig. 9 The optimized molecular structure (a) (the white, dark-blue, light-yellow and light-grey spheres indicate hydrogen, nitrogen, sulfur and carbon atoms, respectively), the MEP (b), HOMO (c) and LUMO (d) electron density of the inhibitor TTHIIDT.

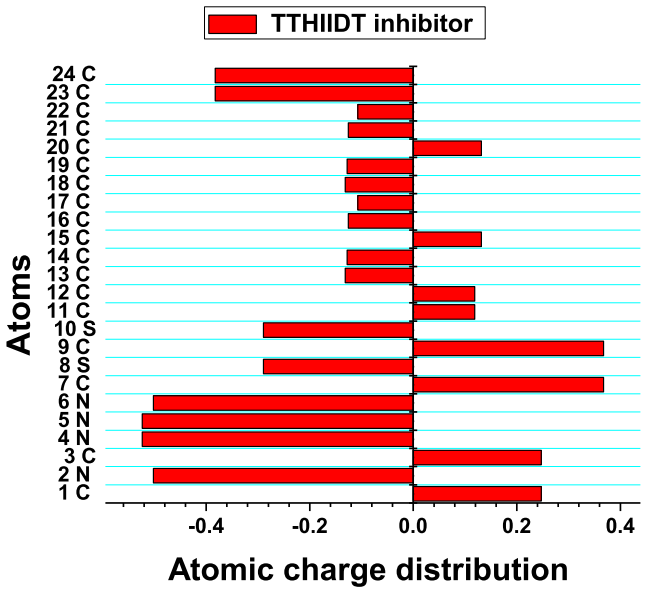

Fig. 10 The atomic charge distribution of the inhibitor TTHIIDT.

behaviour of the investigated inhibitor. These atomic charge distribution analysis results theoretically confirmed that the TTHIIDT molecule has many nucleophilic and electrophilic atoms, which are responsible for its good performance as a good reactive surfactant. Additionally, this inhibitor can adsorb on the surface of carbon steel by chemical and physical adsorption mechanisms.

3.9.2.1. Reactivity descriptor analysis. The molecular descriptors of the inhibitor TTHIIDT, namely, the energy lowest unoccupied molecular orbital's ($E^{DFT}_{LUMO(Inh)}$), the highest occupied molecular orbital's energy ($E^{DFT}_{HOMO(Inh)}$), the energy distinction between LUMO and HOMO energy (ΔE^{DFT}_{Inh}), the molecular ionization potential (I^{DFT}_{Inh}), the electron affinity (A^{DFT}_{Inh}), the electronic chemical potential (μ^{DFT}_{Inh}), the electronic negativity (χ^{DFT}_{Inh}), the chemical hardness (η^{DFT}_{Inh}), the chemical softness (σ^{DFT}_{Inh}), the global electrophilicity index (ω^{DFT}_{Inh}), the nucleophilicity (ε^{DFT}_{Inh}) and the fraction of electron transfer from inhibitor molecule to a carbon steel surface (ΔN^{DFT}_{Inh}), were measured according to Koopmans's theory and Equations (29)–(37) (Chauhan et al., 2020, 2019; Gupta et al., 2019; Chafiq et al., 2020; Bahgat Radwan et al., 2017; Rbaa et al., 2020; Tan et al., 2020a, 2020b; Fan et al., 2019; Kikanme et al., 2020; El Kacimi et al., 2020; Ye et al., 2020; Aly et al., 2020; Tabatabaei majd et al., 2020; Dehghani et al., 2020; Lgaz et al., 2020), as indicated in Table 9.

$$\Delta E^{DFT}_{Inh} = E^{DFT}_{LUMO(Inh)} - E^{DFT}_{HOMO(Inh)} \tag{29}$$

$$I^{DFT}_{Inh} = -E^{DFT}_{HOMO(Inh)} \tag{30}$$

$$A^{DFT}_{Inh} = -E^{DFT}_{LUMO(Inh)} \tag{31}$$

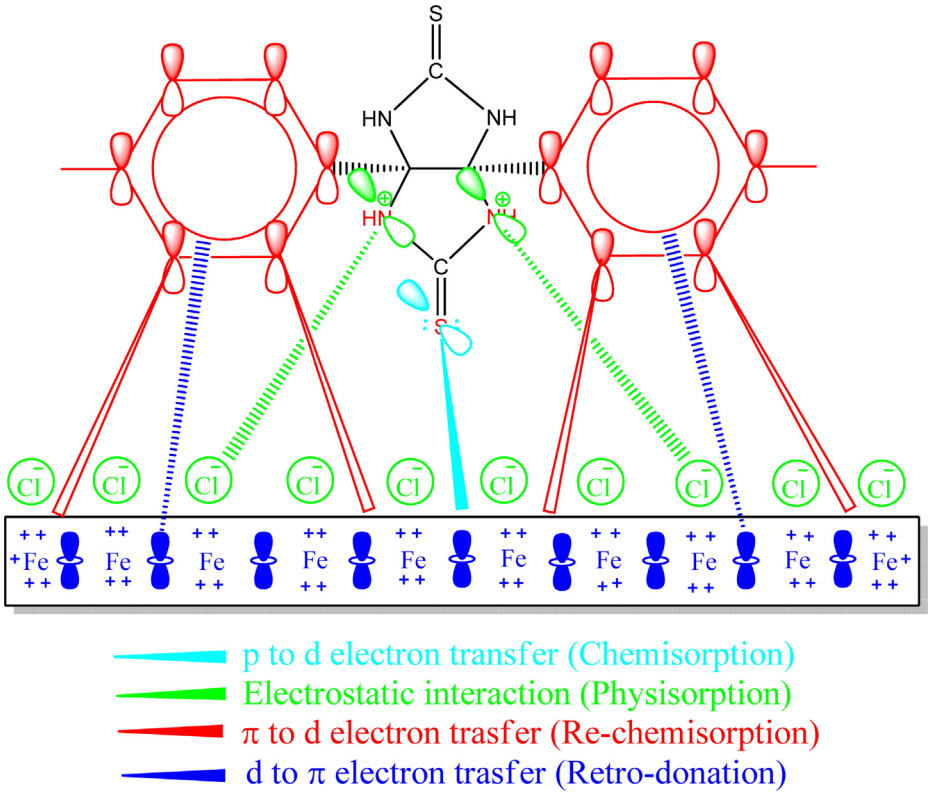

Fig. 11 The pictorial representation of the inhibition mechanism of the TTHIIDT molecule on a carbon steel surface in a HCl environment.

Table 9 The computed reactivity descriptors of the inhibitor TTHIIDT.

Parameters	Value, eV
$E^{DFT}_{LUMO(Inh)}$	−0.032
$E^{DFT}_{HOMO(Inh)}$	−0.211
ΔE^{DFT}_{Inh}	0.179
I^{DFT}_{Inh}	0.211
A^{DFT}_{Inh}	0.032
μ^{DFT}_{Inh}	−0.1215
χ^{DFT}_{Inh}	0.1215
η^{DFT}_{Inh}	0.0895
σ^{DFT}_{Inh}	11.1732
ω^{DFT}_{Inh}	0.0895
ε^{DFT}_{Inh}	12.1212
ΔN^{DFT}_{Inh}	0.3078
Dipole moment, D	8.1

$$-\mu^{DFT}_{Inh} = \chi^{DFT}_{Inh} = \frac{1}{2}(I^{DFT}_{Inh} + A^{DFT}_{Inh}) \tag{32}$$

$$\eta^{DFT}_{Inh} = \frac{1}{2}(I^{DFT}_{Inh} - A^{DFT}_{Inh}) \tag{33}$$

$$\sigma^{DFT}_{Inh} = \frac{1}{\eta} \tag{34}$$

$$\omega^{DFT}_{Inh} = \frac{(\chi^{DFT}_{Inh})^2}{2\eta^{DFT}_{Inh}} \tag{35}$$

$$\varepsilon^{DFT}_{Inh} = \frac{1}{\omega^{DFT}_{Inh}} \tag{36}$$

$$\Delta N^{DFT}_{Inh} = \frac{(\chi_{Fe} - \chi^{DFT}_{Inh})}{2(\eta_{Fe} + \eta^{DFT}_{Inh})} \tag{37}$$

where η_{Fe} is 0 eV mol^{-1} andχ_{Fe} is 7 eV mol^{-1}.

In this investigated work, the global chemical reactivity indicators could be predicted to be related to the LUMO and HOMO energies. The higher and lower energies of the HOMO and LUMO of the studied inhibitor are attributed to the better electron donor and acceptor characteristics, respectively. As observed, the $E^{DFT}_{HOMO(Inh)}$ and $E^{DFT}_{LUMO(Inh)}$ were −0.211 and −0.032 eV, respectively, confirming that the inhibitor TTHIIDT was a more reactive molecule and a better electron donator and acceptor molecule, respectively. This phenomenon confirmed that this inhibitor was an effective adsorbent molecule for the carbon steel surface.

It is remarkable that the studied inhibitor reported a lower ΔE^{DFT}_{Inh} of 0.179 eV and η^{DFT}_{Inh} of 0.0895 eV and a higher σ^{DFT}_{Inh} of 11.1731 eV. This lower η^{DFT}_{Inh} value supports the formation of a lower energetic barrier for electron transfer between inhibitor molecules and Fe atoms, as well as an inner inhibitor molecule, where a higher σ^{DFT}_{Inh} value means the opposite. This phenomenon promotes better interaction behaviour of the studied inhibitor with the surface of carbon steel. As illustrated by the data shown, this inhibitor exhibited a value of 8.1 D; this high dipole moment confirmed TTHIIDT to be a highly polarized molecule, meaning that the positive and negative charges are non-uniformly distributed in the molecule. This highest dipole moment value supports the observation that the inhibitor molecules are more soluble in polarized environments. Next, it should be emphasized that ω^{DFT}_{Inh} and ε^{DFT}_{Inh} were 0.0895 and 12.1212 eV, respectively, suggesting that the studied inhibitor is more nucleophilic and less electrophilic. This result indicates that this inhibitor molecule is attributed to donor electrons to the surface of carbon steel.

From the data shown, it is observed that the investigated inhibitor molecule had a lower electron negative potential; χ^{DFT}_{Inh} was 0.1215 eV, which indicates that the electron is transferred from the studied inhibitor to Fe atoms because this inhibitor's electron negative potential was seven times lower than that of Fe. Another pattern to connect the inhibition behaviour of the observed inhibitor is that ΔN^{DFT}_{Inh} is 0.3078, and it has been reported that the electron transfer behaviour of this inhibitor is the highest; this action promotes effective adsorption.

3.10. Inhibition efficiency comparison with early research

In corrosion science, a study of the inhibition efficiency of different kinds of organic molecules in 1 M HCl solution is conducted, some of which are presented in Table 10 for comparison with the present research work. As observed in Table 10, our inhibitor was more efficient at lower concentrations than the other inhibitors. Another feature aspect illustrates that the inhibitor TTHIIDT could be easily synthesized based on a low-cost local product and that it is biodegradable. This result supports that this inhibitor can be widely used in the chemical industry as an eco-friendly compound.

3.11. Analysis of the inhibition mechanism

The inhibition mechanism of the inhibitor TTHIIDT on the carbon steel surface is illustrated in Fig. 11. It is clear from the image in this figure that this inhibitor can inhibit the car-

Table 10 The comparison of inhibition properties of various inhibitors.

Inhibitors	Corrosive solutions	Inhibitor concentrations	Metal types	η, %	References
HM3	1 M HCl	10^{-6}–10^{-3} mol/L	Mild steel	65–82	(Douche et al., 2020)
SHMB	1 M HCl	0.5 mM	Carbon steel	87.8	(Hany and El-Lateef, 2020)
Q-H	1 M HCl	10^{-6}–10^{-3} M	Mild steel	72.1–92.6	(El Kacimi et al., 2020)
CS-1	1 M HCl	10–200 mg/L	Mild steel	86.80–3.92	
AA2	1 M HCl	10^{-6}–10^{-3} M	Carbon steel	75.2–91	(Dagdag et al., 2020)
TTHIIDT	1 M HCl	50–150 mg/L	Carbon steel	88.03–9.15	Present work

bon steel surface via three stages. First, the protonated nitrogen atoms neutralize the adsorbed Cl^- ions on the surface. Next, physical interactions occur that involve electron donation from the p-electron pairs of sulfur atoms to the vacant 3d-orbitals of Fe atoms. The next step is supplementary electron donation in which the phenyl rings share π-orbitals with vacant 3d-orbitals of Fe, and this process supports chemisorption. The last step is *retro*-donation, which is carried out by electron transfer from the filled Fe orbitals to the vacant anti-bonding π-orbitals in phenyl rings. As concluded, the studied inhibitor molecule could form a self-assembled protective thin layer on the surface of carbon steel, which could isolate the surface from aggressive-corrosive attacks in solution; this phenomenon is accomplished by physical-interaction and chemical-hybridization adsorption activities (Chauhan et al., 2020, 2019; Gupta et al., 2019; Chafiq et al., 2020; Bahgat Radwan et al., 2017; Rbaa et al., 2020; Tan et al., 2020a, 2020b).

4. Conclusion

In this research work, the inhibition behaviours of TTHIIDT for carbon steel in a 1 M HCl environment at various inhibitor concentrations and temperatures were investigated by using gravimetric, EFM, EN, OCP, PDP, EIS, SEM and DFT methods, and the following conclusions were drawn:

1. The inhibition processes of TTHIIDT was fully characterized.
2. The inhibition efficiency of TTHIIDT was over 95–97% and nearly stable in the rise of temperature and concentration.
3. TTHIIDT was mixed type inhibitor and effectively influenced both anodic and cathodic corrosion reactions.
4. The inhibited system has large corrosion and electrochemical noise resistance.
5. TTHIIDT formed the energetic barrier for corrosion processes.
6. A protective hydrophobic thin layer of this inhibitor on the carbon steel surface is more stable and non soluble in 1 M HCl medium.
7. C_{dl} was very low in the inhibited medium than corrosive medium.
8. TTHIIDT controlled the corrosion processes by the charge transfer.
9. This inhibitor adsorbed endothermically on the carbon steel surface by the chemical and physical adsorption processes.
10. The surface morphology is improved the adsorption of TTHIIDT.
11. Quantum chemical calculations supported the experimental results and showed that the inhibition efficiency is depends on the structure of inhibitor.

Declaration of Competing Interest

The authors declare that they have no known competing financial interests or personal relationships that could have appeared to influence the work reported in this paper.

Acknowledgements

The authors wish to acknowledge Tianjin University, School of Chemical Engineering and Technology, Tianjin, P.R. China, and Karshi State University for the support of this research work.

References

Abdel-Rehim, S.S., Khaled, K.F., Abd-Elshafi, N.S., 2006. Electrochemical frequency modulation as a new technique for monitoring corrosion inhibition of iron in acid media by new thiourea derivative. Electrochim. Acta 51, 3269–3277.

Al-Mobarak, N.A., Khaled, K.F., Hamed, Mohamed N.H., Abdel-Azim, K.M., 2011. Employing electrochemical frequency modulation for studying corrosion and corrosion inhibition of copper in sodium chloride solutions. Arabian J. Chem. 4, 185–193.

Aly, Kamal I., Mohamed, Mohamed Gamal, Younis, Osama, Mahross, Mahmoud H., Abdel-Hakim, Mohamed, Sayed, Marwa M., 2020. Salicylaldehyde azine-functionalized polybenzoxazine: synthesis, characterization, and its nanocomposites as coatings for inhibiting the mild steel corrosion. Prog. Org. Coat. 138, 105385.

Bahgat Radwan, A., Sliem, Mostafa H., Okonkwo, Paul C., Shibl, Mohamed F., Abdullah, Aboubakr M., 2017. Corrosion inhibition of API X120 steel in a highly aggressive medium using stearamidopropyl dimethylamine. Molliq. https://doi.org/10.1016/j.molliq.2017.03.116.

Berdimurodov, E., Akbarov, K., Kholikov, A., 2019. Electrochemical frequency modulation and reactivation investigation of thioglycolurils in strong acid medium. Adv. Mater. Res. 1154, 122–128.

Berdimurodov, Elyor, Wang, J., Kholikov, Abduvali, Akbarov, Khamdam, Burikhonov, Bakhtiyor, Umirov, Nurbik, 2016. Investigation of a new corrosion inhibitor cucurbiturils for mild steel in 10% acidic medium. Adv. Eng. Forum, Trans Tech Publ. 18, 21.

Berdimurodov, Elyor, Kholikov, Abduvali, Akbarov, Khamdam, Nakhatov, Innat, Kh Jurakulova, Nigora, Umirov, Nurbek, 2017. Adsorption isotherm and SEM investigating of cucurbit [n] urils based corrosion inhibitors with gossypol for mild steel in alkaline media containing chloride ions. Adv. Eng. Forum, Trans Tech Publ. 23, 13.

Berdimurodov, Elyor, Kholikov, Abduvali, Akbarov, Khamdam, Nuriddinova, D., 2018. Polarization resistance parameters of anti-corrosion inhibitor of cucurbit [N] urils and thioglycolurils in aggressive mediums. Adv. Eng. Forum, Trans Tech Publ. 26, 74.

Bosch, R.W., Hubrecht, J., Bogaerts, W.F., Syrett, B.C., 2001. Electrochemical frequency modulation: a new electrochemical technique for online corrosion monitoring. Corrosion 57 (1), 60–70.

Chafiq, Maryam, Chaouiki, Abdelkarim, Damej, Mohamed, Lgaz, Hassane, Salghi, Rachid, Ali, Ismat H., Benmessaoud, Mohammed, Masroor, Sheerin, Chung, Ill-Min, 2020. J. Mol. Liq. 309, 113070.

Chauhan, D.S., Mazumder, M.A.J., Quraishi, M.A., et al, 2020. Chitosan-cinnamaldehyde Schiff base: A bioinspired macromolecule as corrosion inhibitor for oil and gas industry. Int. J. Biol. Macromol. https://doi.org/10.1016/j.ijbiomac.2020.04.200.

Chauhan, Dheeraj Singh, Quraishi, M.A., Sorour, A.A., Saha, Sourav Kr., Banerjeeb, Priyabrata, 2019. Triazole-modified chitosan: a biomacromolecule as a new environmentally benign corrosion inhibitor for carbon steel in a hydrochloric acid solution. RSC Adv. 9, 14990.

Dagdag, O., Safi, Z., Wazzan, N., et al, 2020. Highly functionalized epoxy macromolecule as an anti-corrosive material for carbon steel: computational (DFT, MDS), surface (SEM-EDS) and electrochemical (OCP, PDP, EIS) studies. J. Mol. Liq. https://doi.org/10.1016/j.molliq.2020.112535.

Danaee, P., Nikparsa, M.R., Khosravi-Nikou, H. Eskandari, Nikmanesh, S., 2019. Density functional theory and electrochemical noise analysis of corrosion inhibition behavior of N, N'-bis(1-(3,5-Dihydroxyphenyl)ethylidene)propane-1,3-diamine on steel in HCl solution. Prot. Met. Phys. Chem. 55 (5), 1001–1014.

Dehghani, Ali, Bahlakeh, Ghasem, Ramezanzadeh, Bahram, Ramezanzadeh, Mohammad, 2020. Potential role of a novel green eco-friendly inhibitor in corrosion inhibition of mild steel in HCl solution: detailed macro/micro-scale experimental and computational explorations. Constr. Build. Mater. 245, 118464.

Douche, Dhaybia, Elmsellem, Hicham, Anouar, El Hassane, Guo, Lei, Hafez, Baraa, Tüzün, Burak, El Louzi, Ahmed, Bougrin, Khalid, Karrouchi, Khalid, Himmi, Banacer, 2020. Anti-corrosion performance of 8-hydroxyquinoline derivatives for mild steel in acidic medium: Gravimetric, electrochemical, DFT and molecular dynamics simulation investigations. J. Mol. Liq. 308, 113042.

Ehsani, A., Mahjani, M.G., Hosseini, M., Safari, R., Moshrefi, R., Mohammad Shiri, H., 2017. Evaluation of Thymus vulgaris plant extract as an eco-friendly corrosion inhibitor for stainless steel 304 in acidic solution by means of electrochemical impedance spectroscopy, electrochemical noise analysis and density functional theory. J. Colloid Interface Sci. 490, 444–451.

El Kacimi, Y., Touir, R., Alaoui, K., Kaya, S., Salem Abousalem, A., Ouakki, M., Ebn Touhami, M., 2020. Anti-corrosion properties of 2-phenyl-4(3H)-quinazolinone-substituted compounds: electrochemical, quantum chemical, Monte Carlo, and molecular dynamic simulation investigation. J. Bio- Tribo-Corros. 6, 47.

Eldesoky, A.M., Hala, M., Hassan, Abdu Subaihi, El Shahawy, Abeer, Farghaly, Thoraya A., 2020. Water pipes corrosion inhibitors for Q235 steel in hydrochloric acid medium using spiropyrazoles derivatives. Coatings 10, 167.

Emoria, Wilfred, Zhang, Run-Hua, Okaforc, Peter C., Zheng, Xing-Wen, Hef, Tao, Weif, Kun, Lin, Xiu-Zhou, Cheng, Chun-Ru, 2020. Adsorption and corrosion inhibition performance of multi-phyto-constituents from Dioscorea septemloba on carbon steel in acidic media: characterization, experimental and theoretical studies. Colloids Surf. A 590, 124534.

Fan, Baomin, Ma, Yucong, Wang, Manman, Hao, Hu.a., Yang, Biao, Lv, Jinyu, Sun, Hui, 2019. Revealing the assembly mechanism of an octadecylamine based supramolecular complex on mild steel in condensate water: correlative experimental and theoretical studies. J. Mol. Liq. 292, 111446.

Gupta, Rajeev Kumar, Manisha Malviya, K.R., Ansari, H., Lgaz, D. S., Chauhan, M.A. Quraishi, 2019. Functionalized graphene oxide as a new generation corrosion inhibitor for industrial pickling process: DFT and experimental approach. Mater. Chem. Phys. 236, 121727.

Hany, M., El-Lateef, Abd, 2020. Corrosion inhibition characteristics of a novel salycilidene isatin hydrazine sodium sulfonate on carbon steel in HCl and a synergistic nickel ions additive: a combined experimental and theoretical perspective. Appl. Surf. Sci. 501, 144237.

Hou, Y., Aldrich, C., Lepkova, K., Machuca, L.L., Kinsella, B., 2016. Monitoring of carbon steel corrosion by use of electrochemical noise and recurrence quantification analysis. Corros. Sci. 112, 63–72.

Hou, B.S., Zhang, Q.H., Li, Y.Y., Zhu, G.Y., Liu, H.F., Zhang, G.A., 2020. A pyrimidine derivative as a high efficiency inhibitor for the corrosion of carbon steel in oilfield produced water under supercritical CO^2 conditions. Corros. Sci. 164, 108334.

Huet, François, Ngo, Kieu, 2019. Electrochemical noise—guidance for improving measurements and data analysis. Corrosion 75 (9), 1065–1073.

Khalaf, Mai M., Tantawy, Ahmed H., Soliman, Kamal A., Hany, M., El-Lateef, Abd, 2020. Cationic gemini-surfactants based on waste cooking oil as new 'green' inhibitors for N80-steel corrosion in sulphuric acid: a combined empirical and theoretical approaches. J. Mol. Struct. 1203, 127442.

Kikanme, N.K., James, A.O., Ngobiri, N.C., 2020. Vigna unguiculata coat extract as green corrosion inhibitor for steel pipeline in HCl. J. Mater. Sci. Res. Rev. 5 (1), 7–20.

Laidler, K.J., 1963. Reaction Kinetics. Pergamon Press, New York.

Lgaz, Hassane, Kr, Sourav, Saha, Abdelkarim Chaouiki, Subrahmanya Bhat, K., Salghi, Rachid, Shubhalaxmi, Priyabrata Banerjee, Ali, Ismat H., Khan, Mohammad I., Chung, Ill-Min, 2020. Exploring the potential role of pyrazoline derivatives in corrosion inhibition of mild steel in hydrochloric acid solution: insights from experimental and computational studies. Constr. Build. Mater. 233, 117320.

Naghizade, Zandi, M.S., Hosseini, S.M.A., 2020. Electrochemical noise analysis of corrosion behaviour of asymmetric electrodes made of mild steel in NaHCO3 solutions at different NaCl concentrations. Measurement. https://doi.org/10.1016/j.measurement.2020.107501.

Obot, I.B., Onyeachu, Ikenna B., 2018. Electrochemical frequency modulation (EFM) technique: theory and recent practical applications in corrosion research. J. Mol. Liq. 249, 83–96.

Obot, I.B., Onyeachu, Ikenna B., Zeino, Aasem, Umoren, S.A., 2019. Electrochemical noise (EN) technique: review of recent practical applications to corrosion electrochemistry research. J. Adhes. Sci. Technol. https://doi.org/10.1080/01694243.2019.1587224.

Ramezanzadeh, B., Arman, S.Y., Mehdipour, M., Markhali, B.P., 2014. Analysis of electrochemical noise (ECN) data in time and frequency domain for comparison corrosion inhibition of some azole compounds on Cu in 1.0 M H_2SO_4 solution. Appl. Surf. Sci. 289, 129–140.

Rauf, A., Mahdi, E., 2012. Evaluating corrosion inhibitors with the help of electrochemical measurements including electrochemical frequency modulation. Int. J. Electrochem. Sci. 7, 4673–4685.

Rbaa, M., Fardioui, M., Verma, C., et al, 2020. 8-Hydroxyquinoline based chitosan derived carbohydrate polymer as biodegradable and sustainable acid corrosion inhibitor for mild steel: experimental and computational analyses. Int. J. Biol. Macromol. https://doi.org/10.1016/j.ijbiomac.2020.03.200.

Saleem Khan, M., Yang, Chunguang, Zhao, Ying, Pan, Haobo, Jinlong Zhao, M., Shahzad, Babar, Kolawole, Sharafadeen Kunle, Ullah, Ihsan, Yang, Ke, 2020. An induced corrosion inhibition of X80 steel by using marine bacterium Marinobacter salsuginis. Colloids Surf., B 189, 110858.

Singh, Mandeep, Parvari, Galit, Botoshansky, Mark, Keinan, Eh.ud., Reany, Ofer, 2014. The synthetic challenge of thioglycolurils. Eur. J. Org. Chem., 933–940

Tabatabaei majd, Mehdi, Naderi, Reza, Ramezanzadeh, Bahram, 2020. Promotion of the active/barrier protection function of epoxy ester coating/steel system utilizing differently synthesized hybrid pigment through zinc acetylacetonate tailored with green inhibitor molecules. Prog. Org. Coat. 138, 105380.

Tan, Jianhong, Guo, Lei, Yang, Hong, Zhang, Fan, El Bakri, Youness, 2020aaaaaa. Synergistic effect of potassium iodide and sodium dodecyl sulfonate on the corrosion inhibition of carbon steel in HCl medium: a combined experimental and theoretical investigation. RSC Adv. 10, 15163.

Tan, Jianhong, Guo, Lei, Dan, Wu., Wang, Shanfei, Rongrong, Yu., Zhang, Fan, Kaya, Savaş, 2020bbbbbb. Electrochemical and computational studies on the corrosion inhibition of mild steel by 1-hexadecyl-3-methylimidazolium bromide in HCl medium. Int. J. Electrochem. Sci. 15, 1893–1903.

Wang, Chen-Xiang, Zhang, Xue-Fen, 2020. A non-particle and fluorine-free superhydrophobic surface based on one-step electrodeposition of dodecyltrimethoxysilane on mild steel for corrosion protection. Corros. Sci. 163, 108284.

Ye, Yuwei, Zou, Yangjun, Jiang, Zilong, Yang, Qiumin, Chen, Liyong, Guo, Shengda, Chen, Hao, 2020. An effective corrosion inhibitor of N doped carbon dots for Q235 steel in 1 M HCl solution. J. Alloy. Compd. 815, 152338.